이학박사 학위논문

다양한 기억상태에서의 성상교세포-기억저장세포 상호작용에 대한 연구

Studies on astrocytic interaction to memory-encoding neurons in varying memory states

2023년 8월

서울대학교 대학원
생명과학부
김 주 영

다양한 기억상태에서의 성상교세포-기억저장세포 상호작용에 대한 연구

지도 교수 강 봉 균

이 논문을 이학박사 학위논문으로 제출함
2023년 8월

서울대학교 대학원
생명과학부
김 주 영

김주영의 이학박사 학위논문을 인준함
2023년 8월

위 원 장	김 형	(인)
부위원장	강봉균	(인)
위 원	이수현	(인)
위 원	고형곤	(인)
위 원	전희정	(인)

Abstract

Studies on astrocytic interaction to memory-encoding neurons in varying memory states

Jooyoung Kim

School of Biological Sciences

The Graduate School

Seoul National University

Memories are stored in subset of memory-encoding neurons, or engrams, that encode, retrieve, and update memory according to experience. Recently, it was shown in behavioral studies that in addition to neurons, astrocyte, the glial cell of the central nervous system, also actively contribute to the encoding of memory. However, it has not been identified how astrocytes interact with memory-encoding neurons to contribute to memory function, due to technical limitations. To examine the question, novel genetically-encoded tool was developed, labeling the interaction between astrocyte and neuron using enhanced GFP reconstitution across synaptic partners (eGRASP). Using the tool, the specific connection of astrocytes to memory-encoding neurons were identified. After the learning, astrocyte connection to memory-encoding neurons were increased. In comparison, after the memory

extinction, astrocyte connection to memory-encoding neurons were decreased, showing that the connection is correlated to memory states. These results strongly suggest that astrocytic connection to memory-encoding neurons is regulated according to memory states, providing the novel mechanism for astrocyte control of memory function.

.....

Keywords: Memory, Astrocyte, Memory-encoding neurons, Synapse

Student Number: 2018-21127

Table of Contents

Abstract iii

List of Figures vi

Chapter 1. Introduction

Background 1

Purpose of this study 7

Chapter 2. Development of astrocyte-eGRASP

Introduction 10

Experimental Procedures 13

Results 18

Discussion 30

Chapter 3. Application of astrocyte-eGRASP in vivo

Introduction 33

Experimental Procedures 37

Results 40

Discussion 51

Chapter 4. Astrocytic interaction to engram neurons correlate memory state

Introduction 55

Experimental Procedures.....57

Results.....61

Discussion.....73

Chapter 5. Conclusion..... 77

Bibliography 80

Abstract in Korean..... 89

List of Figures

Figure 1. DNA constructs for in vitro astrocyte-eGRASP.....19

Figure 2. Astrocyte-eGRASP in primary neuron-primary astrocyte co-culture.....21

Figure 3. Astrocyte-eGRASP reflect dynamics of astrocyte-neuron connection.....23

Figure 4. Application of astrocyte-eGRASP in vivo. 25

Figure 5. Confirmation of astrocyte-eGRASP using CLEM and immunogold EM 27

Figure 6. Application of astrocyte-eGRASP in Striatum.....29

Figure 7. Astrocyte interaction to different compartment of neuron 34

Figure 8. Astrocyte make connection with excitatory and inhibitory neuron.....41

Figure 9. Visualizing astrocyte-dendrite eGRASP with neuronal eGRASP. 43

Figure 10. Astrocyte make connection with pre-synapse and post-synapse.....45

Figure 11. Astrocyte-eGRASP appear on spine and shaft of neuronal dendrite. 47

Figure 12. Astrocyte-eGRASP colocalizes with synaptic and functional proteins.....50

Figure 13. Contextual fear conditioning produce fear memory in mouse. 62

Figure 14. Astrocyte make more connection with engram neurons than nonengram neurons. 64

Figure 15. Dendritic spine with astrocytic connection exhibit larger morphology. 66

Figure 16. Increasing neuronal activity stabilizes astrocytic connection.....68

Figure 17. Extinction decreases fear memory in mouse. 70

Figure 18. Memory extinction reverses increased astrocytic connection to engram neurons. 72

Figure 19 Model for learning-induced changes for astrocyte-neuron connection.....74

CHAPTER I

INTRODUCTION

1.1. Study Background

Memory engram

Memory is encoded by a subset of neurons, called engram neurons (Liu et al., 2012), and the synapses between engram neurons are known as engram synapses (Choi et al., 2021; Choi et al., 2018). Engram neurons are described at several regions important for memory, including amygdala, hippocampus and cortex (Roy et al., 2022). An engram is defined as the physical substrate of memory, and the major properties of engram neurons is that it is activated during learning, store memory, and is reactivated during memory retrieval (Josselyn et al., 2015; Josselyn and Tonegawa, 2020). Inhibiting these subset of memory-encoding neurons impaired memory (Han et al., 2009), while activating it with optogenetic methods retrieved the memory in absence of the conditioned stimuli (Ramirez et al., 2013). Engram neurons are known to have higher excitability than their neighboring neurons (Zhou et al., 2009), and they can be captured post-learning by immediate early gene (IEG) expression. Therefore, doxycycline-dependent tetO system using IEG promoters is used in many memory experiments to tag engram neurons for specific learning session (Ramirez et al., 2013).

Hebbian rule explains how memory is stored in the circuit between memory-encoding neurons. Hebb described the fundamental principle where the synapses between the neurons that fire at the same time is strengthened (Hebb, 1949), which was experimentally proved later in electrophysiology studies. For example, activating presynaptic neuron and postsynaptic neuron in specific time sequence successfully induced the spike-timing dependent plasticity of the connection

between the neurons, including long-term potentiation (Bi and Poo, 1998; Markram et al., 1997). Evidence for the involvement of long-term potentiation in memory was extensively found afterwards. Optogenetic depotentiation of synapses resulted in the disruption of memory (Jeong et al., 2021). Moreover, structural potentiation of specific engram neurons to engram neuron appeared after the learning (Choi et al., 2018), which was dependent of the state of memory (Choi et al., 2021), emphasizing the importance of synaptic plasticity of engram neurons in memory.

The Hippocampus

The hippocampus has long been studied as the site to store episodic memory. The human patient cases with medial temporal lobe lesion (Scoville and Milner, 1957) suggested that the memory function is localized at the certain region of brain. Subsequent animal researches revealed that regions such as hippocampus and amygdala is involved memory encoding (Poldrack and Packard, 2003). Then, specific role of hippocampal subregions including dentate gyrus (DG), Cornu Ammonis (CA) 3 and CA1 and its circuits in memory function was studied. DG is the site of pattern separation (Bakker et al., 2008; Madar et al., 2019) which have been intensively examined in memory reactivation experiments (Liu et al., 2012). CA3 has recurrent collaterals that project to itself, which may participate in the pattern separation and pattern completion (Neunuebel and Knierim, 2014; Vazdarjanova and Guzowski, 2004). CA1 neurons encode temporal (MacDonald et al., 2013) and spatial (O'Keefe and Dostrovsky, 1971) properties of environment, firing at specific timing or at specific location. In addition, hippocampal CA1 astrocytes also show spatial encoding properties (Doron et al., 2022).

Synaptic plasticity in hippocampal pathways have been extensively studied. Hippocampal pathways include mossy fiber pathway (DG-CA3), Schaffer collateral pathway (CA3-CA1), and performant pathway (entorhinal cortex-hippocampus). The long-term potentiation was described in the performant pathway (Bliss and Lomo, 1973) and CA3-CA1 pathway (Wheal et al., 1983), using electrophysiology. Moreover, potentiation of CA3-CA1 synapse has been shown to be involved in memory encoding (Choi et al., 2018).

CA1 receives input from trisynaptic intrahippocampal pathway and performant pathway. CA1 sublayers consist of stratum oriens, stratum pyramidale, stratum radiatum, stratum lacunosum moleculare. Dense pyramidal neuron layers are located at stratum pyramidale. CA3 input to CA1 is mainly located at stratum radiatum and stratum oriens (Ishizuka et al., 1990; Kajiwara et al., 2008), while the performant pathway fibers are mainly located at stratum lacunosum moleculare (Kajiwara et al., 2008).

Astrocytes

Astrocytes are highly abundant glial cells of central nervous system (Pelvig et al., 2008). Astrocyte structure consist of soma, primary branches and distal spongiform processes that may include perisynaptic astrocytic processes (PAPs) or perivascular endfeet (Bushong et al., 2002; Schiweck et al., 2018). More specifically, distal process can be divided into branchlets and leaflets (Gavrilov et al., 2018). Intermediate filaments, such as glial fibrillary acidic protein (GFAP), are present in the soma and main process of astrocyte, while it was not found in spongiform processes (Bushong et al., 2002). Instead, studies suggest that actin cytoskeleton is

involved in the structure of terminal processes dynamics (Schiweck et al., 2018). PAPs show high motility in short time scales, such as in minutes (Bernardinelli et al., 2014).

Owing to neuron doctrine that regards neurons as an unit of information processing (Fodstad, 2002; Golgi, 1906), astrocytes have been only investigated for supportive functions in synaptic communication and cognition for a long time. However, recent studies are revealing that astrocytes are key players of synaptic plasticity and memory.

Astrocytes are directly involved in synaptic communication (Bazargani and Attwell, 2016). Astrocyte responds to neuronal activity (Lezmy et al., 2021; Martin et al., 2015) and can release chemicals (Nishizaki et al., 2002). Increasing astrocyte calcium activity itself could potentiate neighboring synapses (Adamsky et al., 2018; Perea and Araque, 2007). High-resolution imaging proposed that such astrocyte-neuron communication is mediated by the close association of astrocyte and neuron membranes, forming the structures such as tripartite synapse (Araque et al., 1999; Perea et al., 2009). Fine processes of astrocyte enwrap the surface of neuronal membrane (Spacek, 1985), where the distance of interaction could be as small as 10 nm ~ 100 nm (Octeau et al., 2018).

Astrocyte-specific conditional knockout and manipulation tools further revealed its importance in cognitive functions. To date, astrocyte-participating behaviors include, memory encoding (Adamsky et al., 2018; Kol et al., 2020), memory flexibility (Koh et al., 2022), repetitive behaviors (Yu et al., 2018) and hyperactivity (Nagai et al., 2019). Especially, activating hippocampal (Adamsky et al., 2018; Kol et al., 2020) and amygdala (Lei et al., 2022) astrocyte during learning resulted in memory enhancement, showing that astrocyte activity is directly involved

in the memory encoding. In contrast, activating hippocampal astrocyte after learning using channelrhodopsin impaired fear memory (Li et al., 2020), suggesting the complex mechanism of astrocyte action, that would be different to neuron. Also, activation of astrocyte immediately after extinction training facilitated fear extinction, showing that astrocyte is also involved in memory updating (Shelkar et al., 2021).

Structural changes in astrocyte after synaptic modulation and behavioral tests have also been reported. Synaptic potentiation induced increased glial coverage area of spine (Bernardinelli et al., 2014; Lushnikova et al., 2009). In contrast, Badia-Soteras et al. (2022) measured the average distance of astrocytic leaflet to synaptic cleft using EM and found that astrocytic process was transiently retracted from synaptic cleft after learning up to 5 days.

Contextual fear conditioning and extinction

Contextual fear conditioning is one of the Pavlovian classical conditioning (Pavlov, 2010), the behavioral paradigm widely used in memory studies using rodent model animals (Maren, 2001). For contextual fear conditioning, electrical footshock is given to the animal in an unescapable context. Then, the associative memory linking the conditioned stimuli (context) and unconditioned stimuli (footshock) is formed. The memory is evaluated using the fear response of the animal. Among various fear responses, freezing behavior, which is the absence of movement from the animal except the breathing (Grossen and Kelley, 1972), is commonly used to evaluate the fear. Freezing level of the animal is considered to represent the persistence and strength of the associative memory.

Extinction paradigm can be used to measure the updating and removal of

associate memory (Quirk and Mueller, 2008). For extinction, the animal with the associative memory is exposed to the conditioned stimuli without the unconditioned stimuli. By the repeated exposure to the conditioned stimuli, the conditioned response is gradually reduced, representing the elimination of the association of conditioned stimuli and unconditioned stimuli.

In extinction of contextual fear memory, the animal is repeatedly placed in the conditioned context, reducing the freezing level. The extinction can be classified into within-session extinction and between-session extinction. Within-session extinction is the reduction of conditioned response in one session, whereas between-session extinction shows maintained reduction of conditioned response between separate session. The underlying mechanism of within-session and between session extinction is different (An et al., 2017; Choi et al., 2021): within-session extinction is related to the strengthening of inhibitory circuit, while between-session extinction requires multiple extinction sessions and is related to the weakening of existing excitatory circuit, that entails the elimination (Lee et al., 2022) and the structural changes of dendritic spines of engram synapses (Choi et al., 2021).

1.2. Purpose of Research

To find the mechanism of on memory, the molecular, physiological, and morphological properties of engram neurons in the learning process has been examined (Choi et al., 2021; Choi et al., 2018; Han et al., 2007; Jeong et al., 2021; Lee et al., 2022). Recently, it was revealed that astrocyte is an active contributor of memory function (Adamsky et al., 2018; Kol et al., 2020). However, it has not yet been elucidated whether astrocytes interact with engram neurons during memory processing, due to lack of suitable tools. Many studies are using high-resolution imaging technology such as electron microscopy to examine astrocyte-neuron interaction structure. Nanostructure of the astrocyte-neuron interface can be visualized by electron microscopy (Risher et al., 2014); however, limited labeling capacity and the fixation process hinders the investigation of engram neuron-specific astrocyte contact dynamics. Alternatively, fluorescent labeling of membranes can be used (Haber et al., 2006); however, the size of the astrocyte-neuron interface is often under the resolution limit of light microscopy. Therefore, in this thesis, we developed novel tool to visualize astrocyte-neuron contact, and used the newly developed tool to observe the contact dynamics between astrocyte and engram neuron.

In Chapter II, the novel tool, astrocyte-eGRASP, was developed for labeling the astrocyte-neuron connection with fluorescence. The new constructs were subcloned to label the astrocyte-neuron connection with eGRASP method. Next, the functionality of the tool was tested by expressing it in primary neuron – primary astrocyte culture. Then, using live-cell imaging of the fluorescence, it was confirmed that the tool could represent the dynamics of astrocyte-neuron connection. Lastly, the tool was applied in vivo, and confocal and electron microscopy showed that

astrocyte-eGRASP signals appear at astrocyte-neuron interface.

In Chapter III, astrocyte-eGRASP was applied to the in vivo mouse brain to test whether astrocyte-eGRASP could visualize the different types of the astrocytic connection in each sample. Different types of astrocyte-neuron connection were visualized: 1) astrocytic connection to excitatory and inhibitory neurons, 2) astrocytic connection to dendrite with neuronal synapse, 3) astrocytic connection to axon and dendrite, and 4) astrocytic connection to dendritic spine and shaft. Also, the colocalization of astrocyte-eGRASP to synaptic proteins and functional proteins was measured.

In Chapter IV, the astrocytic connection to memory-encoding engram neurons was measured after behavioral training. The density of astrocyte contact to memory-encoding neurons was compared to the contact to random subset of nonengram neurons after contextual fear conditioning. Next, the dendritic spine morphology with and without the astrocytic connection was measured. Then, the astrocytic connection to memory-encoding neurons were examined after the fear memory extinction.

Collectively, in this thesis, the novel tool was developed to visualize the astrocyte-neuron connection and it was shown that astrocytic connection to memory-encoding neuron is specifically involved in the memory encoding and updating.

CHAPTER II

Development of astrocyte-eGRASP

2.1. Introduction

Many neuroscientists accept the notion that structure represents function in nervous system. Such notions may stem from the discovery of neuron doctrine, that was established based on observation of Golgi staining that revealed separate cellular units (Golgi, 1906). From then, technical breakthrough in visualizing brain structure have opened up fundamental questions and answers for the function of nervous system.

In memory research, for example, Choi et al. (2018) recently showed that Hebbian synaptic rules are applied to hippocampal CA3-CA1 synapses in memory encoding, by visualizing the increase of synapses between memory-encoding engram neurons after learning. In other words, synapses of memory circuits are not collectively controlled by the cognitive change, but rather specific subset of synapses are modified to represent the specific memory.

In the field of glia, structural discovery on astrocytic enwrapping neuronal synapses, called tripartite synapses (Araque et al., 1999), has set up the physical basis to understand physiological aspect of astrocyte-neuron communication. Release and receiving of transmitters between astrocyte and neurons have been interpreted to take place at the tripartite synapses (Perea et al., 2009). The group of neuronal synapses enwrapped by a single astrocyte can be the unit of astrocytic regulation, called synaptic islands (Halassa et al., 2007).

Considering the astrocytes' ability to modulate synaptic transmission (Adamsky et al., 2018; Perea and Araque, 2007), how astrocyte affect the subset of synapses from memory-encoding neurons in each synaptic island may reveal the important mechanism for the memory procedure. However, lack of specific tools for

astrocyte-neuron interaction is hindering the identification of the number and types of multiple connections that are made from single astrocyte. High-resolution imaging methods such as EM imaging (Risher et al., 2014) and super-resolution microscopy (Arizono et al., 2020) can be used to measure the interacting domain of astrocyte-neuron accurately, but it is too laborious, time-consuming, and limited in large volumetric imaging to find the specific contact sites of interest. On the other hand, confocal microscopy is more utilizable in imaging astrocyte-neuron interaction (Bernardinelli et al., 2014; Haber et al., 2006), but it has fundamental limitation because astrocytic process can be ultrathin, under the resolution of optical microscopy. To overcome the limitation, development of new techniques is required.

Contact-based fluorescence method could be utilized for labeling astrocyte-neuron interaction for observation in fluorescent microscopy. Recently, the tool called dual-eGRASP have been developed to label neuronal synapses, that allow two fluorescent colors according to the input (Choi et al., 2018). Considering the labeling scale and the large choice of fluorescence colors, eGRASP could be the adequate construct to label astrocyte-neuron contact. Dual-eGRASP utilizes the split ECFP and EYFP, where each segment is expressed in presynaptic terminal and postsynaptic terminal of neuronal synapses. Presynaptic and postsynaptic split fluorescent proteins are reconstituted at the synaptic cleft, labeling it with eGRASP fluorescent, and the colors are determined by the pre-eGRASP compartment. Moreover, the type of postsynaptic neuron could be identified by the fluorescence labeling of the neuronal membrane with myristoylated fluorescent protein.

In this chapter, the new technique called astrocyte-eGRASP was developed by modifying the dual-eGRASP constructs. Instead of expressing pre- and post-eGRASP in synaptic terminals, the constructs were expressed in astrocyte and

neuronal membrane. When astrocyte-eGRASP constructs were expressed in co-culture of primary neuron and primary astrocyte, the reconstituted astrocyte-eGRASP signal appeared at the overlap area of primary neuron and primary astrocyte. Live cell imaging of the astrocyte-eGRASP-expressing co-culture confirmed that the astrocyte-eGRASP fluorescence is reversible, reflecting the dynamics of astrocyte-neuron connection. Also, in vivo functionality of astrocyte-eGRASP was demonstrated at hippocampus and striatum, when it was expressed via adeno-associated virus. Moreover, EM imaging of in vivo astrocyte-eGRASP confirmed that astrocyte-eGRASP labels the site of astrocyte-neuron contact.

2.2. Experimental Procedures

Construction of astrocyte-eGRASP

The glial fibrillary acidic protein (GFAP) promoter was inserted into dual-eGRASP DNA constructs as described in detail by Choi et al. (2018). For the labeling of astrocytes with mBeRFP, mBeRFP was provided by Yang (Yang et al., 2013), and it was subcloned into GFAP-myriRFP-P2A-kSPOPTcSp32Nrx and GFAP-myriRFP-P2A-kSPOPTySp32Nrx.

Mice

For primary culture, postnatal day 2 (P2) and embryonic day 17-18 (E17-18) C57BL/6N mice were purchased from Koatech (Pyeongtaek, South Korea). In vivo astrocyte-eGRASP experiments were performed on 8-to-12-week-old C57BL/6N mice purchased from Samtako. Bio. Korea (Osan, South Korea). Mice were raised under a 12-h light-dark cycle in standard laboratory cages, and food and water were provided ad libitum. All procedures and animal care followed the regulations and guidelines of the Institutional Animal Care and Use Committee of Seoul National University.

Adeno-associated virus production

Adeno-associated viruses serotype 1/2 (AAV1/2; AAV particle containing both serotype 1 and 2 capsids) was packaged as previously described (Choi et al., 2021; Choi et al., 2018). Briefly, AAV1/2 were purified from HEK293T cells that were transfected with plasmids containing each expression cassette flanked by AAV2

ITRs, p5E18, p5E18-RXC1, and pAd-ΔF6. AAV2/1 particles were collected using heparin-agarose suspensions (Sigma, cat. # H6508) or heparin-sepharose resin (Cytiva, cat. # 17099801). The titer was measured by quantitative RT-PCR.

Primary culture

Primary astrocytes were prepared from P2 C57BL/6 mouse pups. The cerebral cortex was dissected from P2 mouse pups and was dissociated using 2.5% trypsin at 37 °C for 30 min and trituration. The dissociated single-cell suspension was plated in a six-well culture plate (SPL, cat# 30006). Cells were grown in an astrocyte culture medium (DMEM supplemented with 15% fetal bovine serum [FBS] and 1% penicillin/streptomycin [Hyclone, cat# SV30010]) at 37 °C in a 5% CO2 incubator. On the third day of culture, the cells were vigorously washed with pipetting, and the medium was replaced to remove other cell types.

For primary neuronal culture, hippocampal tissue was isolated from E17-18 C57BL/6 mouse embryos. The hippocampal tissue was dissociated using 2.5% trypsin at 37 °C for 30 min and trituration in plating media (MEM [Hyclone, cat# sh30024.01] with 10% FBS, 0.45% glucose, 1 mM sodium pyruvate, and 1% penicillin/streptomycin). Dissociated single-cell suspensions were plated in a 24-well culture plate (Thermo Scientific™, cat# 142475) coated with poly-D-lysine. Three hours after plating, the plating medium was removed and replaced with maintenance media (neurobasal medium [Gibco, cat# 21103049] with 2% B27 [Gibco, cat# 17504044], 2 mM GlutaMAX [Gibco, cat# 35050061], and 1% penicillin/streptomycin) at 37 °C in a 5% CO2 incubator.

After AAV transduction, primary astrocytes were detached by

trypsinization and transferred to the primary neuronal culture.

Live cell imaging

For live cell imaging, astrocyte-eGRASP-expressed primary cultures were imaged on an INCell Analyzer 2000 (GE Healthcare, US) with 60x objectives. Cell culture was maintained at 37 °C and CO_2 was supplied during the imaging. Images were obtained at 1-h intervals. We used the FIJI (Schindelin et al., 2012) HyperStackReg plugin (Sharma, 2018) to reconstruct and align images and used Imaris (Bitplane, Zurich, Switzerland) software to label and track astrocyte-eGRASP.

Stereotaxic surgery

Mice (8–10 weeks old) were deeply anesthetized using ketamine/xylazine solution and positioned on a stereotaxic apparatus (Stoelting Co.). The viral mixture was injected into the target regions using a 31-G needle with a Hamilton syringe at a rate of 0.125 μL/min. The total injection volume per site was 0.5 μL, and the needle tip was positioned 0.05 mm below the target coordinate immediately before the injection for 2 min. After injection, the needle was left in place for an additional 7 min before being slowly withdrawn. The stereotaxic coordinates for dorsal CA3 were (AP: -1.7/ ML: ± 2.35/ DV: -2.4), for dorsal CA1 were (AP: -1.8/ ML: ± 1.45/ DV: -1.65 below the skull surface), for dorsal striatum were (AP: +0.5/ ML: ± 2.0 / DV: -3.5) and for nucleus accumbens were (AP: +1.4/ ML: ± 0.65/ DV: -4.5).

Immunogold label electron microscopy (Immuno-EM)

For immuno-EM, mouse brain slices were fixed by 2.5% glutaraldehyde

and 2% paraformaldehyde in sodium cacodylate buffer (pH 7.2) at 4 °C. Samples were fixed in 1% osmium tetroxide (OsO_4) for 30 min at 4 °C. The fixed samples were then dehydrated, performed using an ethanol gradient (50%, 60%, 70%, 80%, 90% and 100%) for 20 min each, and the samples were subsequently transferred to EM812 medium (Electron Microscopy Science, Hatfield, PA, USA). After impregnation with pure resin, specimens were embedded into the same resin mixture. Samples were sectioned (60 nm) with an ultramicrotome (Leica Ultracut UCT; Leica Microsystems, Vienna, Austria) and then collected on nickel grids. Post-embedding immunogold labeling was performed with anti-GFP (Invitrogen, #A-11120) and 9–11 nm colloidal gold conjugated to goat anti mouse IgG secondary antibodies (Sigma-Aldrich, #G7652). Following immunogold labeling, sections were double stained with UranyLess (EMS, #22409) for 2 min and 3% lead citrate (EMS, #22410) for 1 min. Sections were then analyzed using a transmission electron microscope at 120 kV (Tecnai G2, ThermoFisher, USA).

Immunocytochemistry

Cells were rinsed with 1xPBS and fixed with 4% paraformaldehyde and 100% methanol. Cells were washed in 0.1% Triton X-100 with 0.1% BSA in 1xPBS for 15 min and then blocked in 2% BSA with 0.8% Triton X-100 in 1xPBS for 1h at room temperature. Primary anti-GFP (Invitrogen, #A-11120) antibody was applied in blocking solution and incubated overnight at 4°C. The cells were washed two times with 0.1% Triton X-100 with 0.1% BSA in 1xPBS and incubated with secondary antibody (goat anti-mouse Alexa Fluor 488; 1:500 in blocking solution)

for 2 hours at room temperature. Cells were rinsed two times and washed with 0.1% Triton X-100 with 0.1% BSA in 1xPBS and washed two times with 1xPBS

2.3. Results

To develop astrocyte-eGRASP, eGRASP and fluorescent proteins were subcloned in AAV vector (Fig. 1). For astrocyte-specific labeling, the GFAP promoter was utilized. GFAP promoter is commonly used promoter for the expression in astrocytes (O'Carroll et al., 2020). In control of GFAP promoter, myristoylated fluorescent protein was attached to label the astrocytic membrane. Considering the spectrum of eGRASP fluorescence, infrared fluorescent protein (iRFP670v5) and blue-excited RFP (mBeRFP) (Yang et al., 2013) was selected. In downstream of the fluorescence protein, pre-eGRASP was inserted, divided by self-cleaving P2A peptide. As eGRASP was proven to be suitable for labeling synapses, which is supposed to be similar range to astrocyte-neuron interaction (Octeau et al., 2018), no further modification to eGRASP was applied. Astrocyte-eGRASP constructs were made for two colors that are available in eGRASP: cyan and yellow.

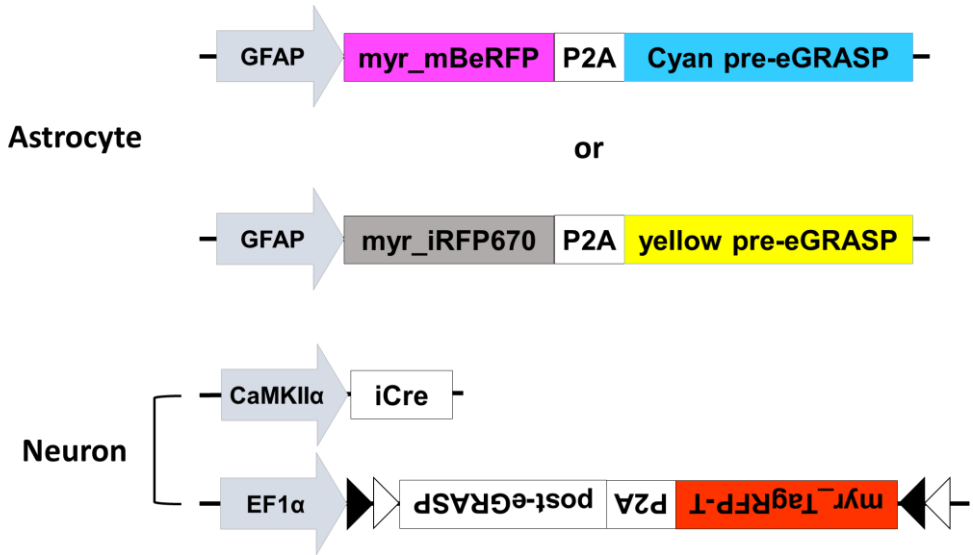

(Collaborated with Dr. Ji-il Kim)

Figure 1. DNA constructs for in vitro astrocyte-eGRASP.

eGRASP DNA constructs were subcloned and inserted into the AAV cassette.

Then, the astrocyte-eGRASP constructs was tested on primary astrocyte-primary neuron co-culture (Fig. 2A). Primary neuron culture and primary astrocyte culture was prepared individually (Fig. 2B), and astrocyte-eGRASP constructs were delivered by AAVs. Myristoylated TagRFP-T and post-eGRASP was expressed in primary neuron culture dependent on CaMKII promoter-driven iCre, and myristoylated mBeRFP and cyan pre-eGRASP was expressed in primary astrocyte culture driven by GFAP promoter. When the primary astrocyte culture was added to the primary neuron culture, cyan eGRASP fluorescence appeared at the overlap region of pre-eGRASP-expressing astrocyte labeled by mBeRFP and post-eGRASP-expressing neuron labeled by TagRFP-T (Fig. 2C). This result showed that eGRASP would be capable for labeling the astrocyte-neuron contact.

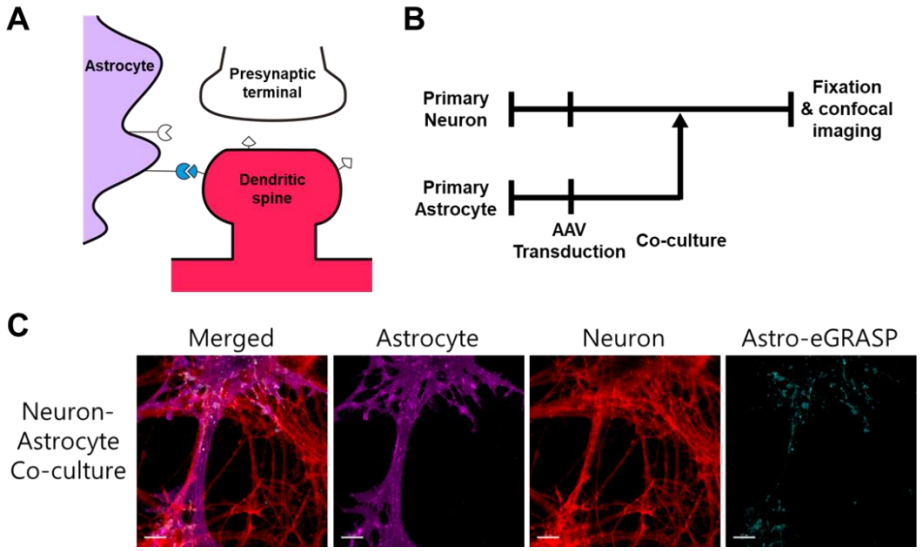

(Collaborated with Jiah Lee and Dr. Heejung Chun)

Figure 2. Astocyte-eGRASP in primary neuron-primary astrocyte co-culture.

(A) Schematic illustration for astrocyte eGRASP.

(B) Experimental procedure for in vitro astrocyte-eGRASP.

(C) Representative image for in vitro astrocyte-eGRASP. Magenta: cyan-eGRASP expressing primary astrocyte. Red: post-eGRASP expressing primary neuron. Cyan: dendrite-astrocyte eGRASP. Scale bar, 10 μm.

Structures of astrocyte-neuron interaction can be more dynamic than neuronal synapses, since astrocyte is extending and retracting in scales of minutes (Haber et al., 2006). So, it is important that labeling with astrocyte-eGRASP is reversible, allowing the appearance and disappearance of astrocyte-neuron contact. To test the reversibility, the live cell imaging was conducted on the primary astrocyte-primary neuron co-culture expressing the astrocyte-eGRASP (Fig. 3A). For the experiment, preparation of the culture was done same as Fig 2., except that yellow pre-eGRASP was expressed in astrocyte, and astrocytic membrane was labeled with myristoylated iRFP. Yellow astrocyte-eGRASP appeared at the overlap region with post-eGRASP-expressing primary neuron labeled by TagRFP-T (Fig. 3B). Between 1-hour timepoint gap, both appearance and disappearance of astrocyte-eGRASP was observed (Fig. 3C). This result show that reconstitution of astrocyte-eGRASP is reversible, indirectly confirming that astrocyte-eGRASP can represent the dynamics of astrocyte-neuron connection.

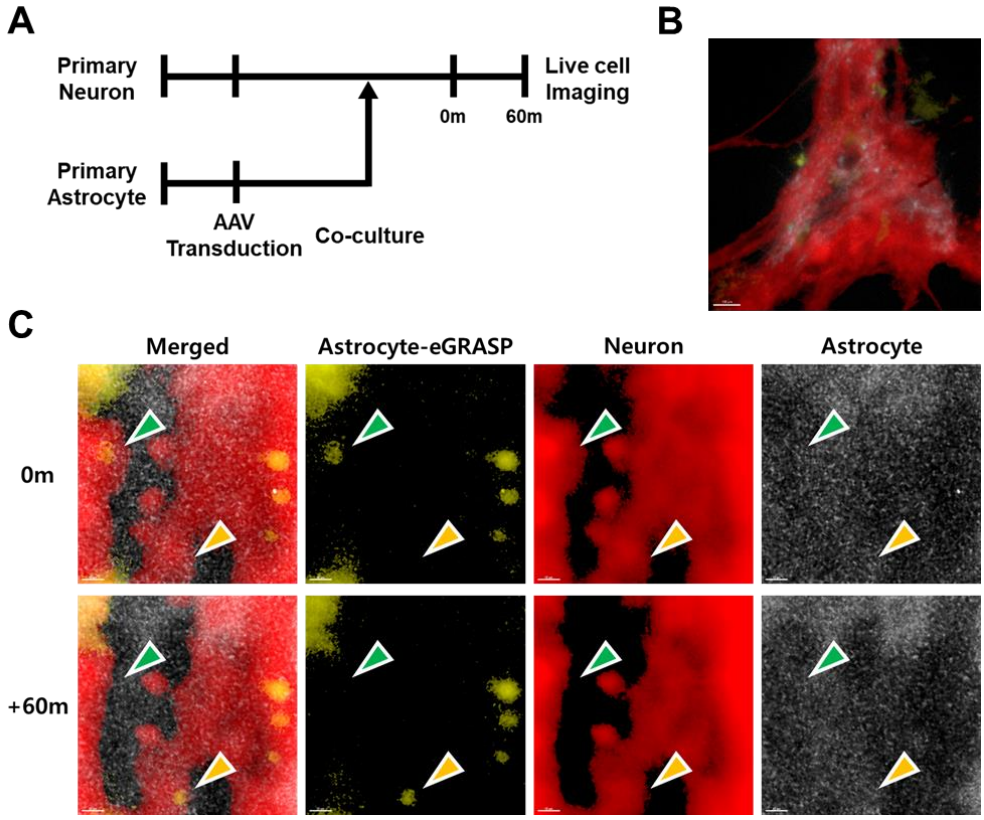

(Collaborated with HyoJin Park)

Figure 3. Astrocyte-eGRASP reflect dynamics of astrocyte-neuron connection.

(A) Experimental procedure for live cell imaging.

(B, C) Representative image for live cell imaging of dendrite-astrocyte eGRASP. Grey: yellow-eGRASP-expressing primary astrocyte. Red: post-eGRASP-expressing primary neuron. yellow: astrocyte-eGRASP. Green arrow: disappearing astrocyte-eGRASP puncta. Yellow arrow: appearing astrocyte-eGRASP puncta. Scale bar, 100 μm (B) and 10 μm (C).

Next, in vivo functionality of astrocyte-eGRASP was tested in the mouse brain. First, yellow astrocyte-eGRASP was expressed in hippocampal CA1 with neuronal eGRASP using AAVs. To compare astrocyte-eGRASP signal to neuronal eGRASP, AAVs containing astrocyte-eGRASP was injected into hippocampal CA1 and AAVs containing neuronal cyan pre-eGRASP was injected into the contralateral hippocampal CA3 (Fig. 4A). Membrane of astrocytes expressing yellow pre-eGRASP was labeled by myristoylated iRFP, which appeared like bush-like morphology in minimally overlapping pattern, as previously described (Bushong et al., 2002). Post-eGRASP was expressed in CA1 excitatory neurons labeled by myristoylated TagRFP-T, while cyan pre-eGRASP was expressed in contralateral CA3 axons (Fig. 4B).

Neuronal eGRASP was expressed within CA3-CA1 circuit, to test if 1) distribution of astrocyte-eGRASP signals are distinct to the distribution of neuronal eGRASP and 2) cyan and yellow eGRASP signals are segregated in the imaging condition. If astrocyte-eGRASP labels the astrocyte-neuron contact, the eGRASP signal will appear only at the overlap region of iRFP-labeled astrocyte and TagRFP-T-labeled neuronal dendrite, while neuronal eGRASP will appear along the CA1 dendrite independent of the astrocytic expression. As expected, yellow eGRASP signals were strictly dependent on the astrocyte territory (Fig. 4C), and cyan eGRASP signals appeared along the dendritic spines as previously described (Choi et al., 2018), regardless of astrocyte territory.

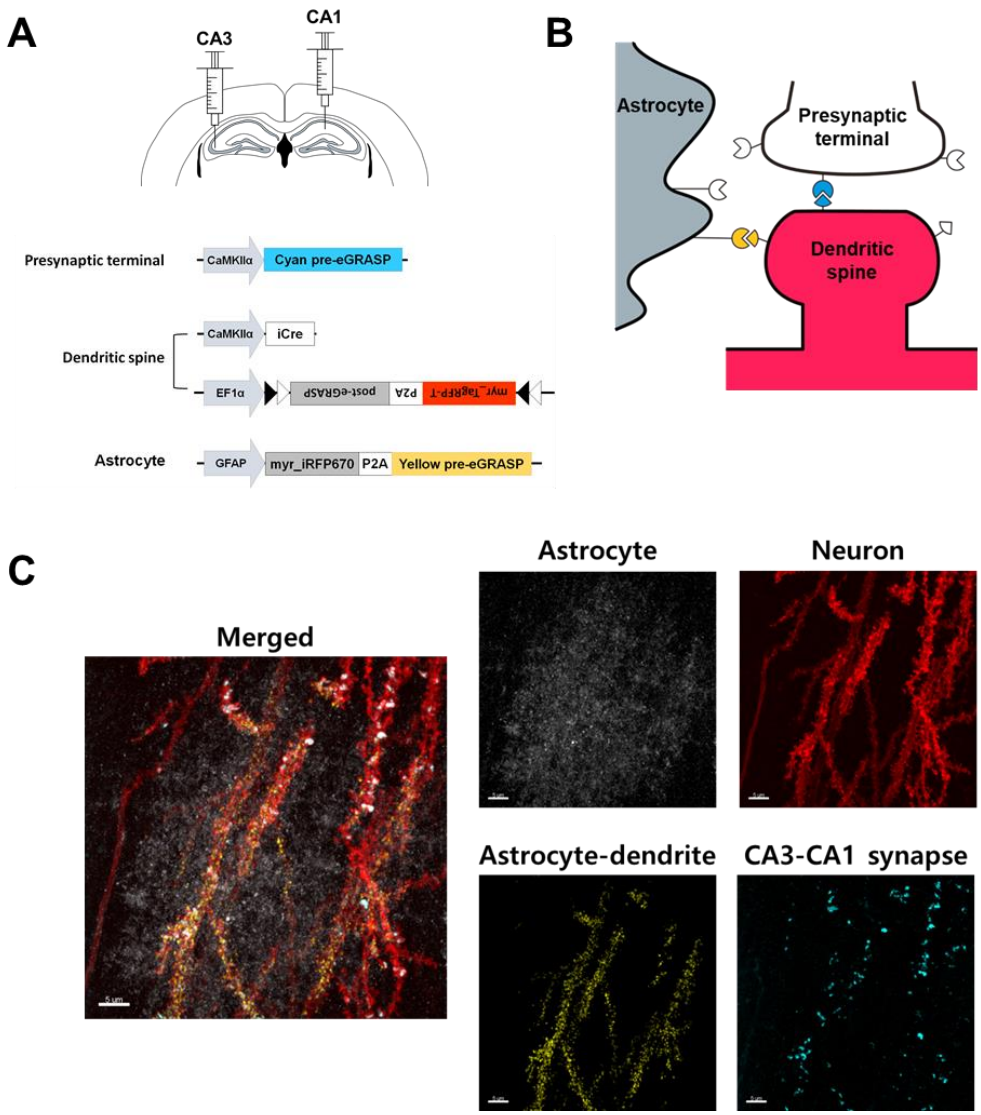

(Collaborated with Dr. Ji-il Kim, Dr. Dong Il Choi)

Figure 4. Application of astrocyte-eGRASP in vivo.

(A, B) Virus combination and schematic illustration for dendrite-astrocyte eGRASP with CA3-CA1 neuronal eGRASP.

(C) Representative image for dendrite-astrocyte eGRASP with CA3-CA1 neuronal eGRASP. Grey: yellow pre-eGRASP-expressing astrocyte. Red: post-eGRASP-expressing dendrite. Cyan: CA3-CA1 neuronal eGRASP. Yellow: dendrite-astrocyte eGRASP. Scale bar, 5 μm.

It is important to confirm if the new technique is actually labeling the astrocyte-neuron contact. In collaboration with Korea Brain Research Institute, the immunogold EM was conducted to find the location of astrocyte-eGRASP reconstitution. Prior to that, the antibody labeling reconstituted GFP (Zhang et al., 2016) was tested by immunocytochemistry of neuron culture co-expressing pre-eGRASP and post-eGRASP compared with that of neuron culture expressing either pre-eGRASP or post-eGRASP (Fig. 5A). Then, astrocyte-eGRASP was expressed in the mouse hippocampal CA1, using the same viral combination as in Fig. 4A, and it was labeled with the immunogold. EM imaging of the astrocyte-eGRASP confirmed that immunolabeled eGRASP signals appear at the astrocyte-neuron interface (Fig. 5B).

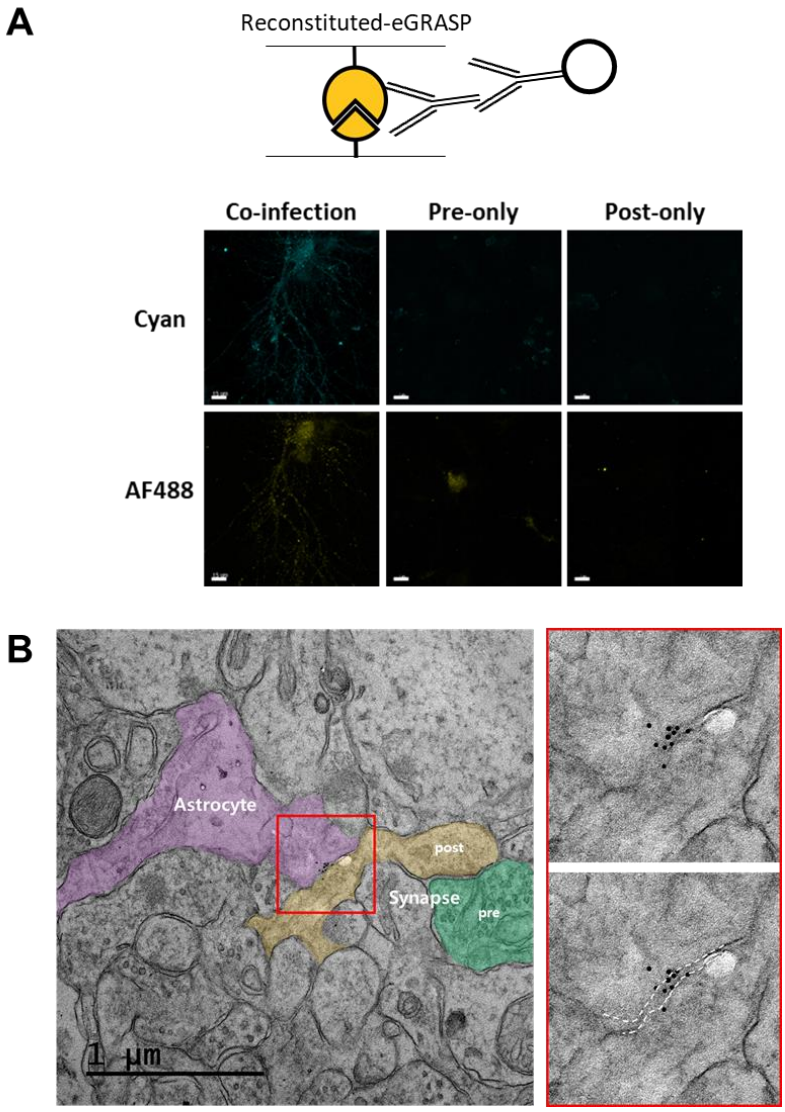

(Collaborated with Dr. Minkyo Jung, Hoonwon Lee, Seoulgi Noh, Dr. Ji Young Mun)

Figure 5. Confirmation of astrocyte-eGRASP using CLEM and immunogold EM

(A) Antibody test for capturing the reconstituted eGRASP. Scale bar, 15 μm.

(B) Immunogold EM image for astrocyte-eGRASP. White dotted line represents astrocyte and neuronal membrane.

Moreover, it was tested whether astrocyte-eGRASP can be used in brain regions other than hippocampus. To find out, AAVs delivering astrocyte-eGRASP was injected into dorsal striatum and nucleus accumbens. Striatum is one of the regions where astrocyte is known to affect neuronal activity importantly (Khakh, 2019; Martin et al., 2015). Yellow astrocyte-eGRASP appeared at the interface of iRFP-labeled astrocyte and TagRFP-T-labeled neurons in both dorsal striatum (Fig. 6A) and nucleus accumbens (Fig. 6B). These results show that astrocyte-eGRASP technique can be widely applied for in vitro and in vivo studies.

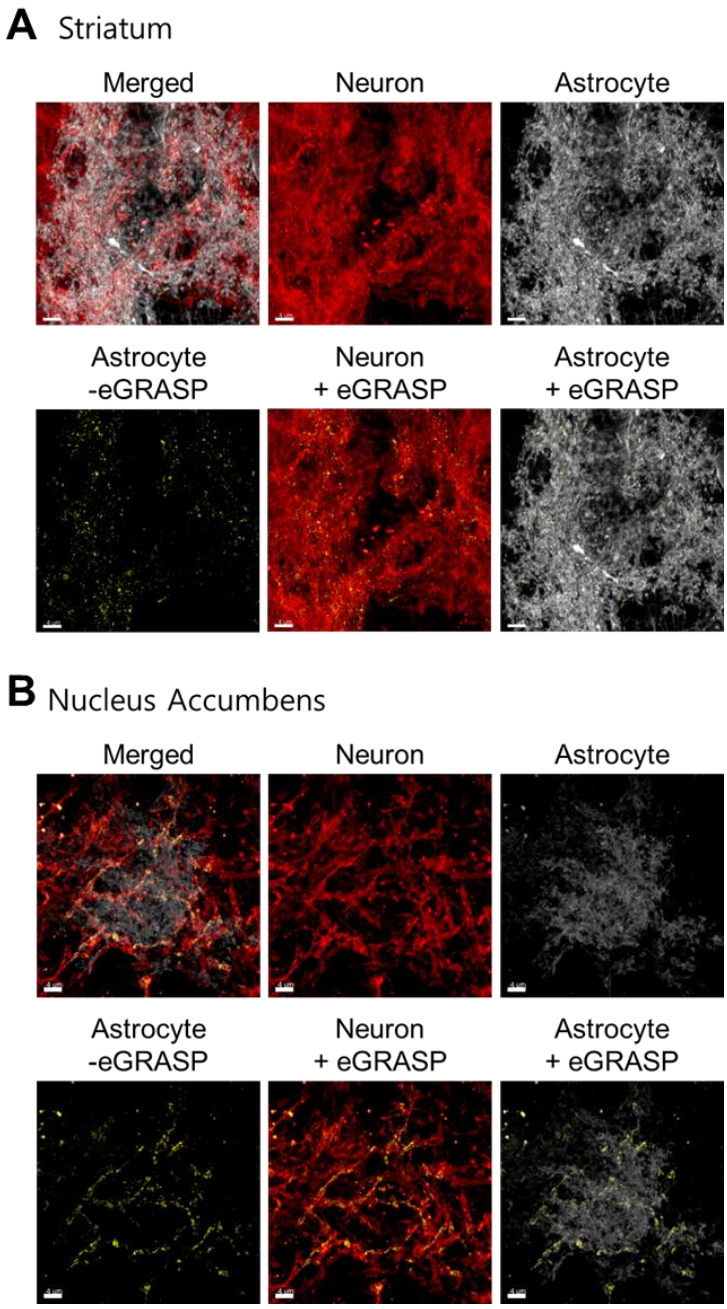

(Collaborated with Dr. Dong Il Choi)

Figure 6. Application of astrocyte-eGRASP in striatum.

A) Representative image for astrocyte-eGRASP in striatum. Scale bar, 4 μm.

(B) Representative image for astrocyte-eGRASP in nucleus accumbens. Scale bar, 4 μm.

2.4. Discussion

In this chapter, the new technique, astrocyte-eGRASP was developed and confirmed. The astrocyte-eGRASP constructs were expressed at the membrane of astrocyte and neuron respectively, and the eGRASP signals appeared at the overlapping region of the astrocyte and the neuron. Live cell imaging of the astrocyte-eGRASP-expressing co-culture confirmed that astrocyte-eGRASP reconstitution is reversible, potentially reflecting the dynamics of the astrocyte-neuron contact. Also, in vivo functionality of astrocyte-eGRASP was demonstrated in various brain regions, such as hippocampus and striatum. EM imaging confirmed that astrocyte-eGRASP appears in between astrocyte and neuronal membrane.

Astrocyte-eGRASP signals appeared all over where the neuron overlaps astrocyte territory. Each astrocyte-eGRASP signals appear as punctate shape in fluorescence imaging, reflecting the nature of astrocyte-neuron contact, in which fine processes of astrocyte associate with the neuron. Punctate appearance of astrocyte-eGRASP allow the quantification of the connection, making the measurement of astrocyte-neuron interaction easier compared to the previous tools, where distance of astrocytic process to neuronal membrane had to be measured to determine the contact.

Astrocyte-eGRASP is the readily available technique to visualize and analyze the astrocyte-neuron interaction within each astrocyte territory. Astrocyte is known to make connection to various types of neurons in large number. Astrocyte-eGRASP has the potential to be used to identify the types of each astrocyte-neuron connection, that will open up the opportunity to study the detailed role of synaptic island of the astrocyte and astrocytic interaction to each subcellular compartment of the neurons. Also, appearance and disappearance of astrocyte-eGRASP showed that

it can reflect the dynamics of astrocyte-neuron contact. Combining astrocyte-eGRASP with the live cell or in vivo fluorescent imaging will provide the platform to perform the long-term in vivo tracking experiments, that may reveal the mechanism astrocyte-neuron interaction during cognitive function or pathophysiology of astrocyte-related diseases.

CHAPTER III

Application of astrocyte-eGRASP in vivo

3.1. Introduction

Astrocytes are exposed to diverse neuronal signals by different types of astrocyte-neuron contacts in vivo brain. Astrocyte-neuron contact is heterogenous in both anatomical and functional properties (Volterra et al., 2014). Astrocytes minimally overlap with each other in many brain regions including hippocampus (Bushong et al., 2002), so the group of synapses in the occupied domain is regulated by single astrocyte. This group of synapses in territory of one astrocyte was named 'synaptic islands' (Halassa et al., 2007), but we will use the term 'astrocytic island' instead in this thesis, because recent reports suggest that astrocyte may also interact with extrasynaptic membrane as well (Gavrilov et al., 2018; Patrushev et al., 2013). Astrocyte is known to mediate hetero-neuronal plasticity induced by neuronal depolarization (Martin et al., 2015; Navarrete and Araque, 2010), suggesting that the astrocytic island may be functional unit of astrocytic regulation. Single astrocyte is estimated to interact with hundred-thousand number of synapses in hippocampus (Bushong et al., 2002), that may come from different neurons. In addition, each neuron will belong to multiple astrocytic domains, making astrocyte-neuron interaction more complex.

Astrocytes interact with different compartment of neurons (Fig 7), including synaptic terminals forming tripartite synapses and non-synaptic dendritic shaft domain (Gavrilov et al., 2018). Also, within tripartite synapse, astrocyte may interact with axon-spine interface, with presynaptic terminals, or with postsynaptic terminals respectively (Aten et al., 2022; Gavrilov et al., 2018; Witcher et al., 2007). Astrocytic activity is affected by presynaptic mechanism (Perez-Alvarez et al., 2014) and postsynaptic mechanism (Navarrete and Araque, 2010).

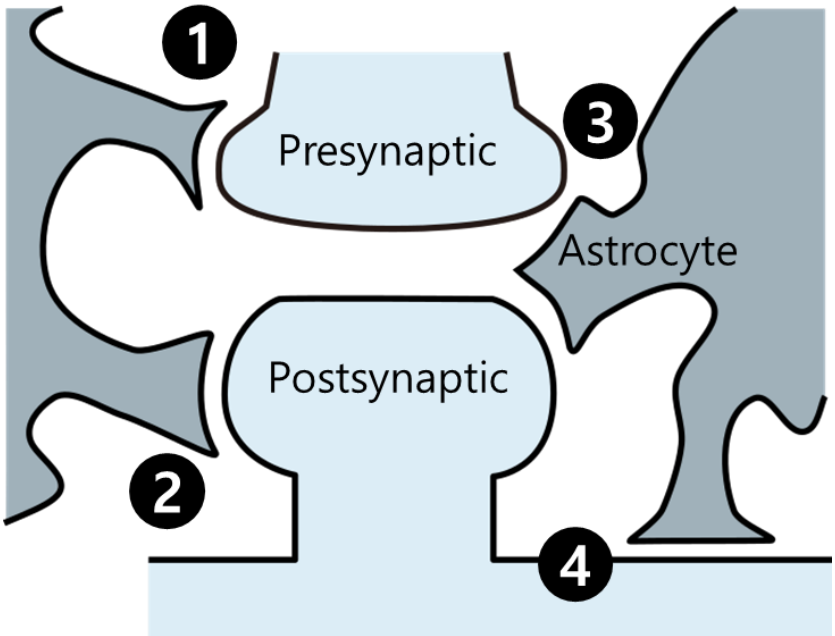

Figure 7. Astrocyte interaction to different compartment of neuron

Schematic illustration for astrocyte-presynaptic terminal (1), astrocyte-postsynaptic terminal (2), astrocyte-axon-spine interface (3) and astrocyte-shaft (4) connection.

Lastly, spatial interaction and dynamics of astrocyte vary depending on the subtypes of synapses (Octeau et al., 2018), and possibly the molecular component. Octeau et al. (2018) analyzed astrocyte-neuron connection in striatum using fluorescence resonance energy transfer (FRET)-based approach, and found that astrocyte show different proximity to dopaminergic and glutamatergic synapses. Interestingly, it was reported that astrocyte regulate neurons and synapses with different subtypes in specific manner (Kruyer et al., 2022; Martin-Fernandez et al., 2017; Martin et al., 2015), suggesting that astrocyte can discriminate the types of cells they are interacting with in their astrocytic island.

To understand the structural-functional heterogeneity of astrocyte-neuron interaction, it is fundamental to identify the complex astrocyte-neuron contact structure. Especially, considering that the group of contacts in each astrocytic island is regulated together, it would be important to distinguish the diverse type of astrocyte-neuron contact in each astrocyte territory. However, such studies have been lacking, due to technical difficulties. Newly developed tool, astrocyte-eGRASP can be used to overcome the problem, that can be used to visualize the distinct types of astrocyte-neuron interaction in single astrocyte territory.

In this chapter, astrocyte-eGRASP was applied in vivo to visualize different types of astrocyte-neuron contacts in astrocytic island and tested the colocalization of molecular components. To visualize astrocyte connection to different neuronal cell types in astrocytic island, astrocyte-excitatory neuron and astrocyte-inhibitory neuron connection was labeled with yellow and cyan astrocyte-eGRASP. To visualize tripartite synapses, astrocyte-eGRASP was expressed with neuronal eGRASP, and astrocyte-axon and astrocyte-dendrite connection was identified with astrocyte-eGRASP. Also, molecular property of the contact labeled by astrocyte-

eGRASP was identified with the immunolabeling. These results provide that astrocyte-eGRASP is readily available tool to visualize the astrocytic contact on different types of synapses and membrane, that would pave the way for the future discoveries on complex astrocyte-neuron interactions.

3.2. Experimental Procedures

Construction of plasmids

To express post-eGRASP in astrocyte, pre-eGRASP in GFAP-myriRFP-P2A-kSPOPTcSp32Nrx and GFAP-myrmBeRFP-P2A-kSPOPTySp32Nrx was replaced with post-eGRASP. To express pre-eGRASP in dendrite, pre-eGRASP was subcloned into EF1a-DIO-myrmScarlet-I-P2A-post-eGRASP, replacing post-eGRASP, and the transmembrane domain was replaced with Neuroligin transmembrane domain with deletion (transmembrane domain of post-eGRASP from Choi et al. (2018)).

Mice

All experiments were performed on 8-to-12-week-old C57BL/6N mice purchased from Samtako. Bio. Korea (Osan, South Korea). Mice were raised under a 12-h light-dark cycle in standard laboratory cages, and food and water were provided ad libitum. All procedures and animal care followed the regulations and guidelines of the Institutional Animal Care and Use Committee of Seoul National University.

Adeno-associated virus production

Adeno-associated viruses serotype 1/2 (AAV1/2; AAV particle containing both serotype 1 and 2 capsids) was packaged as previously described (Choi et al., 2021; Choi et al., 2018). Briefly, AAV1/2 were purified from HEK293T cells that were transfected with plasmids containing each expression cassette flanked by AAV2

ITRs, p5E18, p5E18-RXC1, and pAd-ΔF6. AAV2/1 particles were collected using heparin-agarose suspensions (Sigma, cat. # H6508) or heparin-sepharose resin (Cytiva, cat. # 17099801). The titer was measured by quantitative RT-PCR.

Stereotaxic surgery

Mice (8–10 weeks old) were deeply anesthetized using ketamine/xylazine solution and positioned on a stereotaxic apparatus (Stoelting Co.). The viral mixture was injected into the target regions using a 31-G needle with a Hamilton syringe at a rate of 0.125 μL/min. The total injection volume per site was 0.5 μL, and the needle tip was positioned 0.05 mm below the target coordinate immediately before the injection for 2 min. After injection, the needle was left in place for an additional 7 min before being slowly withdrawn. The stereotaxic coordinates for dorsal CA3 were (AP: -1.7/ ML: ± 2.35/ DV: -2.4) and for dorsal CA1 were (AP: -1.8/ ML: ± 1.45/ DV: -1.65 below the skull surface).

Image analysis

We used the Imaris software (Bitplane, Zurich, Switzerland) to process the confocal images. eGRASP signal was labeled as a sphere using Imaris spot function before they were manually counted.

Immunohistochemistry

Brain sections were rinsed three times in 1xPBS. Sections were blocked in 1xPBS with normal goat serum and TritonX-100 for 1 hour at room temperature. Sections were incubated in primary antibodies rabbit anti-Nrx1 (Invitrogen; PA5-

79764; 1:500), rabbit anti-NL2 (Synaptic Systems; 129 203; 1:500), rabbit anti-PSD95 (Invitrogen; 51-6900; 1:100), rabbit anti-Gephyrin (Synaptic Systems; 147 008; 1:200), rabbit anti-MCT2 (Alomone Labs; AMT-012; 1:200), rabbit anti-MCT4 (Sigma-Aldrich; AB3314P; 1:100), mouse anti-GluR2 (Sigma-Aldrich; MAB397; 1:500) in blocking solution at 4℃ overnight. Sections were rinsed three times with 1xPBS. Sections were incubated in secondary antibody (goat anti-rabbit Alexa Fluor 488; A-11034; 1:500, goat anti-mouse Alexa Fluor 488; 1:500 in blocking solution) for 2 hours at room temperature. Sections were rinsed three times with 1xPBS. For PSD95 and Gephyrin, sections were pre-treated with 0.5% TritonX-100 for 30 minutes before primary antibody treatment. For GluR2, sections were pre-treated with goat anti-mouse IgG (Abcam; ab6668; 1:50) for 1 hour before the primary antibody treatment.

3.3. Results

Structural identification of astrocyte-neuron connection in single astrocyte territory had been hindered due to the lack of utilizable tool. While it is known that astrocyte interact with various subtypes of neurons (Khakh, 2019; Mederos and Perea, 2019), there is lack of structural reports showing that single astrocyte is interacting with different subtypes of neurons simultaneously. In this context, it was questioned whether the newly developed fluorescent tool, astrocyte-eGRASP, could label the astrocyte contact with dendrites of different neuronal subtypes. Therefore, astrocyte-eGRASP was expressed in excitatory and inhibitory neurons of the hippocampus (Fig. 8A). To visualize connection to both excitatory neurons and inhibitory neurons in the same astrocyte territory, double-floxed inverted open reading frame (DIO) system was used with iCre and Flippase recombinases. post-eGRASP was expressed in astrocyte using GFAP promoter, yellow pre-eGRASP in excitatory neurons using CaMKII-iCre, and cyan pre-eGRASP in inhibitory neurons using mDlx-Flippase. As a result, yellow eGRASP appeared at the excitatory dendrite and cyan eGRASP appeared at the inhibitory dendrite, where they meet astrocyte (Fig. 8B). It is notable that yellow and cyan eGRASP signals appeared in same astrocyte territory, structurally confirming that single astrocyte island interacts with different cell types of neurons.

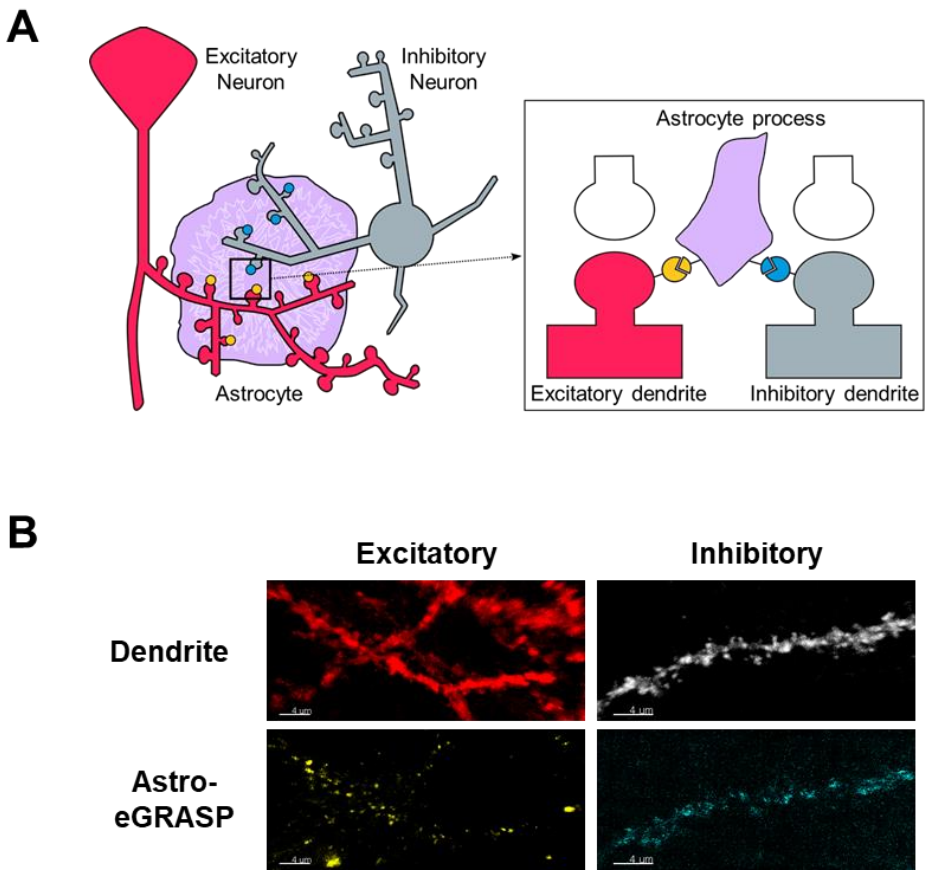

(Collaborated with Dr. Ji-il Kim, Dr. Dong Il Choi)

Figure 8. Astrocyte make connection with excitatory and inhibitory neuron.

(A) Schematic illustration for astrocyte-eGRASP constructs expression at excitatory and inhibitory neurons.

(B) Representative image for astrocyte-eGRASP on excitatory and inhibitory neurons. Red: yellow pre-eGRASP-expressing dendrite of the excitatory neuron. Grey: cyan pre-eGRASP-expressing dendrite of the inhibitory neuron. Yellow: dendrite-astrocyte eGRASP between excitatory neuron and astrocyte. Cyan: dendrite-astrocyte eGRASP between inhibitory neuron and astrocyte. Scale bar, 4 μm.

To test whether astrocyte-eGRASP can visualize different types of astrocyte-neuron contacts located on different compartments of neuron, the contacts within tripartite synapse was visualized with eGRASP first. eGRASP is developed in two colors, so two connections of tripartite synapses were visualized in each combination. Firstly, closer imaging of astrocyte-eGRASP expressed with neuronal eGRASP was conducted, using the sample from the chapter I, Fig. 4. Briefly, astrocyte-eGRASP was injected at hippocampal CA1, and neuronal pre-eGRASP was injected at contralateral CA3 (Fig. 9A), labeling neuronal synapses with cyan-eGRASP and astrocyte-neuron contact with yellow-eGRASP (Fig. 9B). Cyan eGRASP and yellow eGRASP signals appeared besides each other at some of the dendritic spine head (Fig. 9C), showing that astrocyte-eGRASP can label astrocyte-postsynaptic terminal connection within the tripartite synapses.

Closer examination revealed that astrocyte-eGRASP appeared at the head and the neck of dendritic spines, and also at the dendritic shafts, as a punctate shape. It is consistent with the previous descriptions that astrocytes interact with neurons with fine peri-astrocytic processes, that may enwrap the synapses or shaft partially (Gavrilov et al., 2018; Witcher et al., 2007). Also, neuronal eGRASP mostly appeared at the head of dendritic spine as previous report (Choi et al., 2018), while cyan and yellow eGRASP signals were separated well. It is reflecting that astrocyte process do not interfere with the synaptic cleft (Rollenhagen et al., 2007). It also excludes the possibility that neuronal and astrocyte-eGRASP signals affect the appearance of each other, due to the clustering of post-eGRASP.

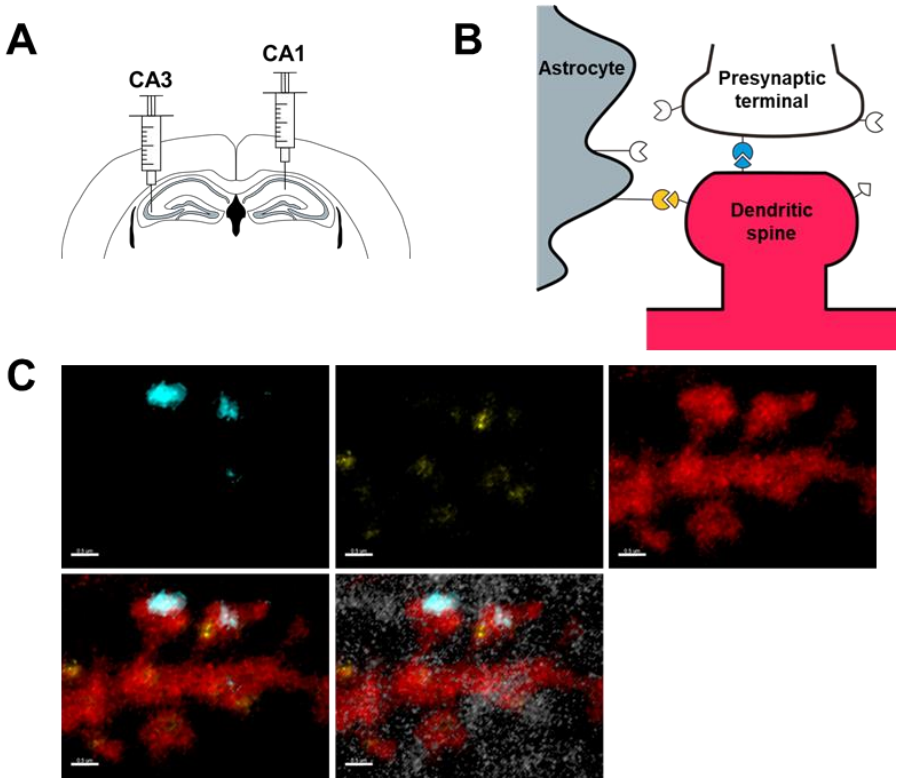

(Collaborated with Dr. Ji-il Kim, Dr. Dong Il Choi)

Figure 9. Visualizing astrocyte-dendrite eGRASP with neuronal eGRASP.

(A) Injection site of astrocyte-eGRASP and neuronal eGRASP.

(B) Schematic illustration of astrocyte-eGRASP and neuronal eGRASP.

(C) Representative image for astrocyte-eGRASP and neuronal eGRASP. Grey: yellow pre-eGRASP-expressing astrocyte. Red: post-eGRASP-expressing dendrite. Cyan: CA3-CA1 neuronal eGRASP. Yellow: dendrite-astrocyte eGRASP. Scale bar, 0.5 μm.

Next, visualization of astrocytic interaction to presynaptic and postsynaptic terminals of excitatory synapses using astrocyte-eGRASP was attempted. Astrocytes can establish contact with presynaptic and postsynaptic terminal independently (Witcher et al., 2007), so it is expected that astrocyte contact to presynaptic and postsynaptic terminal would partially overlap. For the experiment, new astrocyte-eGRASP construct expressing post-eGRASP in astrocyte was made. Also, neuronal counterpart expressing yellow pre-eGRASP at the dendrite was newly developed. The two new constructs were expressed at the hippocampal CA1, combined with expression of cyan pre-eGRASP at contralateral CA3 neurons (Fig. 10A). As a result, yellow astrocyte-eGRASP labeling dendrite-astrocyte contact and cyan astrocyte-eGRASP labeling axon-astrocyte interaction appeared at the territory of the iRFP-labeled astrocyte (Fig. 10B, C). On some dendritic spine, yellow astrocyte-eGRASP appeared at the side of the spine head, while cyan astrocyte-eGRASP appeared at the presumable opposite side of the synapse, where the axonal bouton is expected to be present (Fig. 10C). The yellow and cyan eGRASP signals appeared right beside each other on those dendritic spines, indicating that the astrocyte was interacting to the axon-spine interface. Also, a few cyan neuronal eGRASP signals overlapped with the yellow astrocyte-eGRASP signal at the dendritic shafts, suggesting that some of the shaft astrocyte-eGRASP is labeling immature excitatory synapses on the dendritic shaft (Reilly et al., 2011).

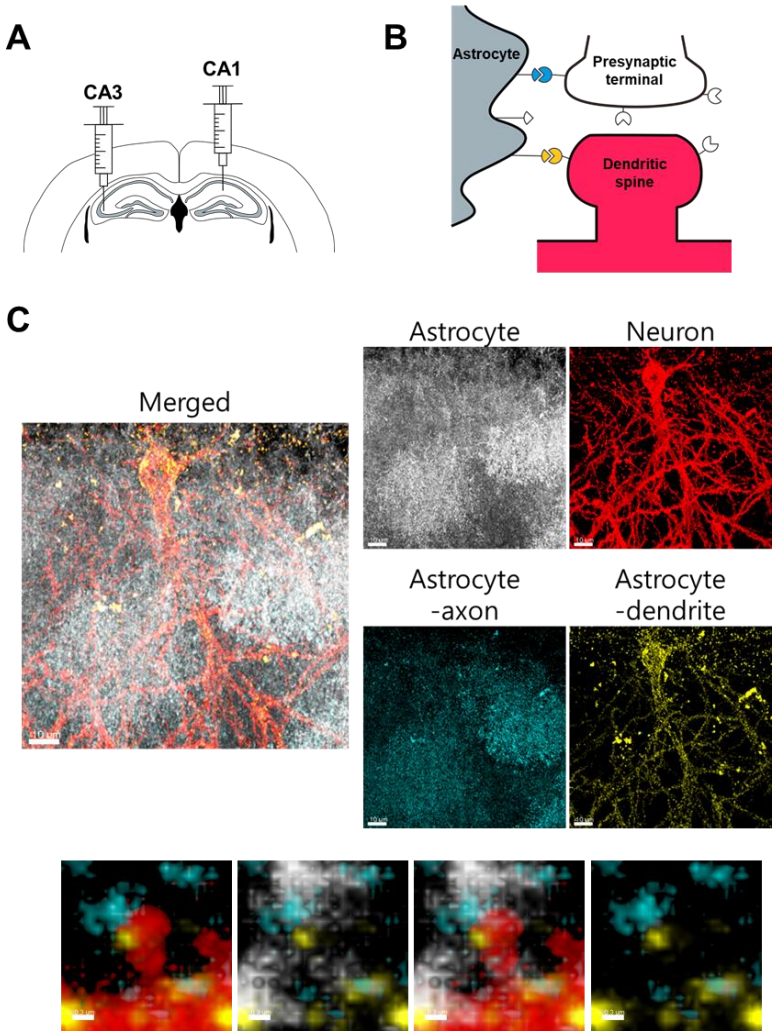

(Collaborated with Dr. Ji-il Kim, Dr. Dong Il Choi)

Figure 10. Astrocyte make connection with pre-synapse and post-synapse.

(A, B) Injection site and schematic illustration for axon-astrocyte and dendrite-astrocyte eGRASP.

(C) Representative image for axon-astrocyte and dendrite-astrocyte. Grey: post-eGRASP-expressing astrocyte. Red: yellow pre-eGRASP-expressing CA1 dendrite. Cyan: axon-astrocyte eGRASP. Yellow: dendrite-astrocyte eGRASP. Scale bar, 10 μm (top) and 0.3 μm (bottom).

For identification of astrocyte-dendritic shaft contact, TagRFP-T was expressed in neurons with yellow astrocyte-eGRASP in the hippocampal CA1 (Fig. 11A). Confocal microscopy revealed that considerable percentage of astrocyte-eGRASP appeared on not only the head and neck or dendritic spines, and also on the dendritic shafts (Fig. 11B, C) More interestingly, larger percentage of astrocyte-eGRASP was on spine in secondary/tertiary dendrite compared to the dendritic trunk (Fig. 11D). The difference in astrocyte-eGRASP distribution suggests that the influence of astrocyte may work differently on the dendritic trunk and secondary/tertiary dendrite as well. Such interpretation is consistent with previous study that astrocytic regulation is compartmentalized in neurons (Ashhad and Narayanan, 2016).

Interaction of astrocytic processes on dendritic spine head and neck has been frequently reported (Witcher et al., 2007), while report of astrocytic interaction on the shaft of dendrites (Gavrilov et al., 2018) or inhibitory synapse (Brunskine et al., 2022) has been relatively scarce, since it is difficult to identify contact with less characteristic shapes using previous tools. The result shows that astrocyte-eGRASP is a strong tool to visualize the different types of contact to neuronal dendrite, readily revealing previously underestimated astrocyte contact located on the dendritic shafts.

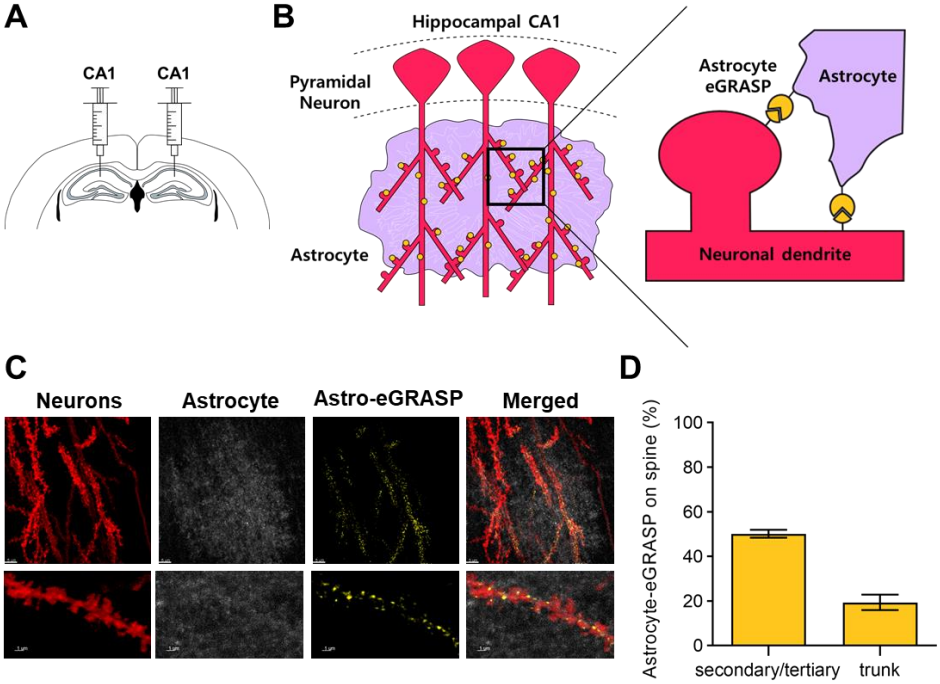

(Collaborated with Dr. Ji-il Kim, Sanghyun Ye)

Figure 11. Astrocyte-eGRASP appear on spine and shaft of neuronal dendrite.

(A, B) Injection site and schematic illustration for astrocyte-eGRASP.

(C) Representative image for astrocyte-eGRASP in CA1. Grey: yellow pre-eGRASP-expressing astrocyte. Red: post-eGRASP-expressing dendrite. Yellow: dendrite-astrocyte eGRASP. Scale bar, 5 μm (top) and 1 μm (bottom).

(D) Ratio of astrocyte-eGRASP on spine and shafts in secondary/tertiary dendrite or dendritic trunk. Secondary/tertiary dendrite, n =12; Trunk, n = 8. Data are represented as mean ± SEM.

Next, it was tested whether astrocyte-eGRASP colocalizes with the synaptic proteins. Cyan astrocyte-eGRASP was expressed in hippocampal CA1, and immunolabeling of the molecules was conducted. Astrocyte-eGRASP showed 18.73±2.129% overlap with Nrx1 and 14.76±2.198% overlap with NL2 (Fig. 12A) Nrx1 is known to be localized at the presynaptic terminal (Klatt et al., 2021; Pregno et al., 2013), and NL2 is known to be localized at the postsynaptic terminal of inhibitory (Varoqueaux et al., 2004) and cholinergic (Takacs et al., 2013) synapses. Also, astrocyte-eGRASP showed 19.83±3.576% overlap with PSD95 and 7.95±2.197% overlap with gephyrin (Fig. 12B). These results suggest that around one-fifth proportion of astrocyte contact is colocalizing with excitatory synapses, while around 8% of astrocyte contact is colocalizing with inhibitory synapses and cholinergic synapses respectively.

Then, it was tested whether astrocyte-eGRASP overlap with MCT transporters of astrocyte-neuron lactate shuttle, through which astrocyte provides energy to neuron (Bergersen, 2007; Mason, 2017). Although neuron-expressed MCT2 is known to be mainly located at the postsynaptic density of excitatory synapses and dendritic spines (Bergersen et al., 2005), the exact location of lactate shuttle is not clear (Pierre and Pellerin, 2005). MCT2 overlapped with 7.861±1.223% of astrocyte-eGRASP, and MCT4, that are expressed in astrocytes, overlapped with 32.6±2.581% of astrocyte-eGRASP (Fig. 12C). Larger percentage of astrocyte-eGRASP overlapping with MCT4 than the synaptic adhesion proteins may suggest that extrasynaptic astrocytic contact may play other functions than modulating synaptic communication.

Lastly, it was tested whether astrocyte is overlapping with neurotransmitter

receptor, such as AMPA receptor. GluR2 subunit of AMPA receptor was visualized with immunofluorescence and the colocalization with astrocyte-eGRASP was counted. GluR2 overlapped with 27.62±3.478% of astrocyte-eGRASP (Fig. 12D). The overlap percentage with GluR2 is similar but larger than the overlap with PSD95, possibly because of the extrasynaptic AMPA receptors (Borgdorff and Choquet, 2002).

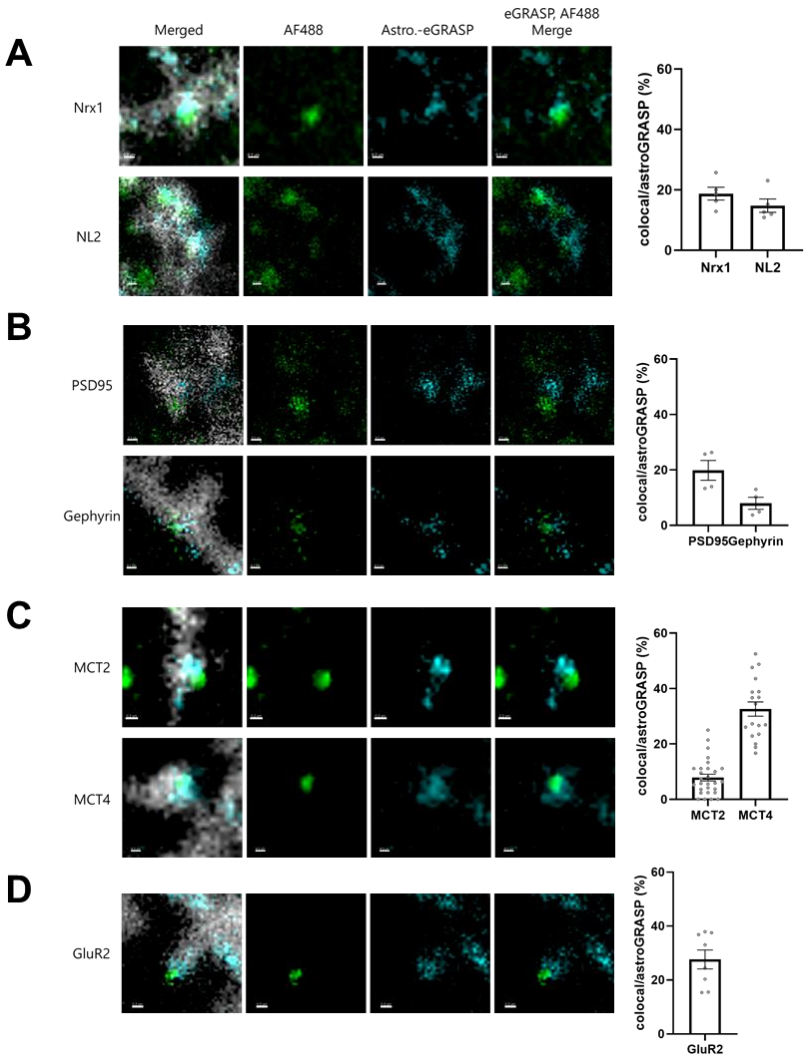

(Collaborated with Yongmin Sung, HyoJin Park)

Figure 12. Astrocyte-eGRASP colocalizes with synaptic and functional proteins. Astrocyte-eGRASP (cyan) colocalizes with immunolabeled signal (green) of synaptic cell adhesion molecules (A), postsynaptic scaffolding proteins (B), MCTs (C) and GluR2 (D). Nrx1, n = 5; NL2, n = 5; PSD95, n = 4; Gephyrin, n = 4; MCT2, n = 28; MCT4, n = 18; GluR2, n = 8. Data are represented as mean ± SEM. Scale bar, 0.2 μm.

3.4. Discussion

In this chapter, the astrocyte connections to dendrites and axons of excitatory neuron and dendrites of inhibitory neuron were identified with astrocyte-eGRASP. The result clearly shows that single astrocyte make connection to different compartments and various subtypes of neurons, and that newly developed tool astrocyte-eGRASP can visualize the various types of astrocyte-neuron connection. Single astrocyte can make connection with excitatory and inhibitory neurons, which could be visualized with different colors of eGRASP. Applying astrocyte-eGRASP to CA3 axon and CA1 dendrite explicitly visualized that astrocyte connection to axon and dendrite separately. Moreover, the connection between astrocyte and hippocampal CA1 pyramidal neurons was visualized which revealed that astrocyte make connection to both dendritic spines and shafts, in different proportions than previously known.

Using astrocyte-eGRASP, the ratio of astrocyte contact to dendritic spine and dendritic shaft was measured, revealing that considerable percentage of astrocytic contacts are located outside the dendritic spine. Also, it was found that dendritic trunks have more denser astrocyte-eGRASP on shafts than secondary/tertiary dendrites. It was previously known that astrocyte may cover neuronal compartments other than the excitatory synapses (Gavrilov et al., 2018), but it attained relatively little attention and the importance was underestimated. It was possibly due to the fact that previous tools were incapable of measuring the overall contact while tracking the dendrite. Astrocyte-eGRASP identifies the precise number of contacts on each labeled dendrite within each astrocyte, offering the advantage of wide field of view of fluorescent microcopy.

Studies on astrocytic contact other that on excitatory synapses are relatively

lacking, so the exact distribution and role of each astrocyte-shaft contact types on cognitive functions are not clear. Shaft astrocyte-eGRASP may include inhibitory tripartite synapses, immature excitatory synapses, or astrocytic contact to dendritic shafts, that may block the crosstalk between synapses (Patrushev et al., 2013).

Although structural description of astrocyte contact to inhibitory synapses are lacking (Brunskine et al., 2022), it is well known that astrocyte interact with inhibitory signaling (Matos et al., 2018). In the result, it has been shown that astrocyte-eGRASP overlaps with Gephyrin and Neuroligin2, that constitute inhibitory synapses. The overlap with Neuroligin2 was slightly larger than the overlap with gephyrin. NL2 is located at cholinergic synapses as well (Takacs et al., 2013), which suggest that the overlap with Neuroligin2 may include the neuromodulatory tripartite synapse as well.

Astrocyte is involved in the generation of immature excitatory synapses on the dendritic shafts (Risher et al., 2014). Excitatory synapses on the dendritic shaft can be the indication of synaptogenesis (Bourne and Harris, 2011; Reilly et al., 2011), which is an important mechanism of the memory formation process (Lee et al., 2022). During visualizing CA3 to CA1 neuronal eGRASP with astrocyte-eGRASP, it was observed that some of the overlapped signals were on the dendritic shafts, suggesting that astrocyte-eGRASP on dendritic spines may include the immature excitatory synapses. Astrocytes may participate in the shaft-to-spine transition of excitatory synapses (Risher et al., 2014), indicating that astrocyte contact on immature synapses may play an important role in spine maturation. Future studies should investigate the role of astrocyte-shaft connection in cognition.

The percentage of colocalization to Nrx1 and PSD95 was lower than the percentage of astrocyte-eGRASP on dendritic spine. It may be because that not all

dendritic spines are synapses, and that synaptic adhesion molecules and scaffold proteins are presumably located at the axon-spine interface, so astrocyte-eGRASP on the side and neck of dendritic spine would not colocalize with the signal. These results suggest that astrocyte contact may be distributed over different areas of synapses, and considerable number of contacts are made at the extrasynaptic region.

Astrocyte-eGRASP revealed its usefulness in visualizing astrocyte-axon and astrocyte-dendrite connection in single astrocyte. Astrocyte-axon interaction is less studied than astrocyte-dendrite interaction, but physiological studies suggest that astrocyte interact with dendrite and axon in separate routes. In hippocampus, astrocyte interacting with axon-spine interface is major, but some synapses have astrocyte contact with only either presynaptic terminals or postsynaptic terminals (Witcher et al., 2007). Recently, astrocyte was shown to control axon conduction via adenosine signaling (Lezmy et al., 2021). Future studies should identify and examine the role of each interaction types of astrocyte-neuron contacts.

CHAPTER IV

Astrocytic interaction to engram neurons correlates memory state

4.1. Introduction

Synaptic structure is the physical site of CNS communication. Correlation between the strength of synapses and its structure has long been studied. Long-term potentiation, the physiological correlate of learning, results in emergence (Engert and Bonhoeffer, 1999) and enlargement of dendritic spines (Fortin et al., 2010; Matsuzaki et al., 2001), making the structure of dendritic spine an indicator for synaptic plasticity. More recently, investigation of synaptic structure on memory-encoding engram neurons, that are physical correlate of memory (Josselyn et al., 2015), was conducted. It has been revealed that density and morphology of engram synapses, synapses between engram neurons, are increased after learning (Choi et al., 2021; Choi et al., 2018). Moreover, synaptogenesis and spine turnover of engram neurons were shown to be involved with learning and memory (Lee et al., 2022). In addition, the morphology of the dendritic spine of engram synapses is correlated to the state of memory (Choi et al., 2021), confirming the linkage of the synaptic structure and memory. Thus, understanding the synaptic structure will be the important step to fully understand the mechanism of synaptic action in CNS information processing.

Astrocyte is known to be related to synaptic structure and cognitive function. It was repeatedly shown that astrocytes and its releasable factors are involved in synaptogenesis (Christopherson et al., 2005). Also, astrocyte mediate phagocytosis of synapses after the exposure to environmental change (Lee et al., 2021). In addition, the stability and morphology of synapses were shown to be related with the coverage by astrocytic processes (Bernardinelli et al., 2014; Haber et al., 2006).

Moreover, astrocytes are involved in memory encoding and updating. It

was shown that modulating astrocytic calcium activity could enhance (Adamsky et al., 2018; Kol et al., 2020; Lei et al., 2022) or impair the episodic memory (Li et al., 2020), though the results varied depending on the tool used. Also, knockout of astrocytic molecules resulted in memory (Gao et al., 2016) and memory updating (Koh et al., 2022) impairments. These results show that astrocytes are important factor of memory function, possibly participating in the memory-encoding neurons' modulation. However, astrocytic communication with memory-encoding neurons and its synapses is yet to be elucidated.

In this chapter, the connection between astrocyte and memory-encoding engram neurons was visualized using astrocyte-eGRASP. In hippocampal CA1, the density of astrocyte-eGRASP was compared between engram neurons and neighboring nonengram neuron within the same astrocyte territory after contextual fear conditioning and extinction. After learning, astrocyte contacts to engram neurons were increased. In addition, the spine morphology was larger in the dendritic spine with astrocyte connection than in the dendritic spine without astrocyte connection. Activating neurons in primary astrocyte-primary astrocyte co-culture with bicuculline increased the stability of astrocyte connection, suggesting that astrocytic process surrounding the engram neurons may be affected by the neuronal activity during learning. Moreover, astrocyte connection to engram neurons was decreased to the control level after the memory extinction, demonstrating that astrocytic contact to engram neurons is dependent on the state of memory. These results suggest that during learning, activity of engram neurons increases its connection to astrocyte, and its persistence is dependent on the state of memory.

4.2. Experimental Procedures

Mice

All behavioral experiments were performed on 8-to-12-week-old C57BL/6N mice purchased from Samtako. Bio. Korea (Osan, South Korea). Mice were raised under a 12-h light-dark cycle in standard laboratory cages, and food and water were provided ad libitum. All procedures and animal care followed the regulations and guidelines of the Institutional Animal Care and Use Committee of Seoul National University.

Adeno-associated virus production

Adeno-associated viruses serotype 1/2 (AAV1/2; AAV particle containing both serotype 1 and 2 capsids) was packaged as previously described (Choi et al., 2021; Choi et al., 2018). Briefly, AAV1/2 were purified from HEK293T cells that were transfected with plasmids containing each expression cassette flanked by AAV2 ITRs, p5E18, p5E18-RXC1, and pAd-ΔF6. AAV2/1 particles were collected using heparin-agarose suspensions (Sigma, cat. # H6508) or heparin-sepharose resin (Cytiva, cat. # 17099801). The titer was measured by quantitative RT-PCR.

Stereotaxic surgery

Mice were deeply anesthetized using ketamine/xylazine solution and positioned on a stereotaxic apparatus (Stoelting Co.). The viral mixture was injected into the target regions using a 31-G needle with a Hamilton syringe at a rate of 0.125 μL/min. The total injection volume per site was 0.5 μL, and the needle tip was

positioned 0.05 mm below the target coordinate immediately before the injection for 2 min. After injection, the needle was left in place for an additional 7 min before being slowly withdrawn. The stereotaxic coordinates for dorsal CA3 were (AP: -1.7/ ML: ± 2.35/ DV: -2.4) and the coordinate for dorsal CA1 was (AP: -1.8/ ML: ± 1.45/ DV: -1.65 below the skull surface).

Contextual fear conditioning

All mice were fear-conditioned 2–4 weeks after the AAV injection. Each mouse was single caged 7 days before conditioning and habituated to the hands of the investigator and anesthesia chamber without isoflurane for 5 days. On the conditioning day, 250 μL of 5 mg/mL doxycycline solution dissolved in saline was injected intraperitoneally 2 hours prior to the conditioning, under brief anesthesia using isoflurane. For contextual fear conditioning, mice were placed in the fear conditioning chamber (Med Associates Inc.), and after 150 s, three electrical foot shocks were given (2 s, 0.75 mA). Approximately 30 s after the last foot shock, mice were returned to their home cages. One day after conditioning, the mice were placed in the conditioned context to measure their freezing behavior. Freezing behavior was recorded and scored using VideoFreeze software (Med Associates Inc.).

For fear extinction, fear conditioned mice were placed in the conditioned context for 30 minutes for 2 days. For control, mice in homecage group was kept in their homecages while mice in extinction group went through extinction. One day after the last extinction, the mice in both extinction and homecage group were placed in the conditioned context to measure their freezing behavior. Freezing behavior was recorded and scored using VideoFreeze software (Med Associates Inc.).

Image analysis

We used the Imaris software (Bitplane, Zurich, Switzerland) to process the confocal images. Each image was cropped at the boundary of a single astrocyte using the Imaris surface function. Each trackable fluorescent protein-labeled dendrite was manually denoted as a filament, during which other fluorescent signals were hidden to exclude any bias. Each cyan or yellow eGRASP signal was labeled as a cyan or yellow sphere.

For eGRASP density analysis, the number of denoted cyan or yellow spheres was manually counted along each denoted filament. Normalization of the eGRASP density was performed within each astrocyte using the average eGRASP on iRFP-labeled dendrites within each image. For spine morphology analysis, each dendrite and dendritic spine were reconstructed in 3D by Imaris filament function.

Statistical analysis

All statistical analyses were performed using Prism 9 (GraphPad). Non-normal datasets were compared using a two-tailed Mann-Whitney test. The exact value of the sample size and statistical significance are reported in each figure legend.

Live cell imaging

For live cell imaging, astrocyte-eGRASP-expressed primary cultures were imaged on an INCell Analyzer 2000(GE Healthcare, US) with 60x objectives. Cell culture was maintained at 37 °C and CO_2 was supplied during the imaging. Images were obtained before and after bicuculline treatment. Images were obtained at 1-h

intervals. We used the FIJI (Schindelin et al., 2012) HyperStackReg plugin (Sharma, 2018) to reconstruct and align images and used Imaris (Bitplane, Zurich, Switzerland) software to label and track astrocyte-eGRASP.

4.3. Results

To label and express eGRASP in engram neurons, myristoylated mScarlet-I and post-eGRASP was expressed under the control of TRE promoter, that is activated by fos promoter-driven rtTA in presence of doxycycline. For internal control, post-eGRASP and myristoylated iRFP was expressed in random population of excitatory neurons, using iCre recombinase. Yellow pre-eGRASP and mBeRFP was expressed in astrocyte, so that astrocyte-neuron contact was labeled with yellow astrocyte-eGARSP signal in both engram and nonengram neurons. Cyan pre-eGRASP was expressed in contralateral CA3 axon. To capture fear memory engram, contextual fear conditioning was conducted, while injecting doxycycline 2-hours prior to the conditioning, and the freezing level was tested one day later (Fig. 13A). Freezing levels for mice used for astrocyte-eGRASP analysis appeared reliably high (Fig. 13B).

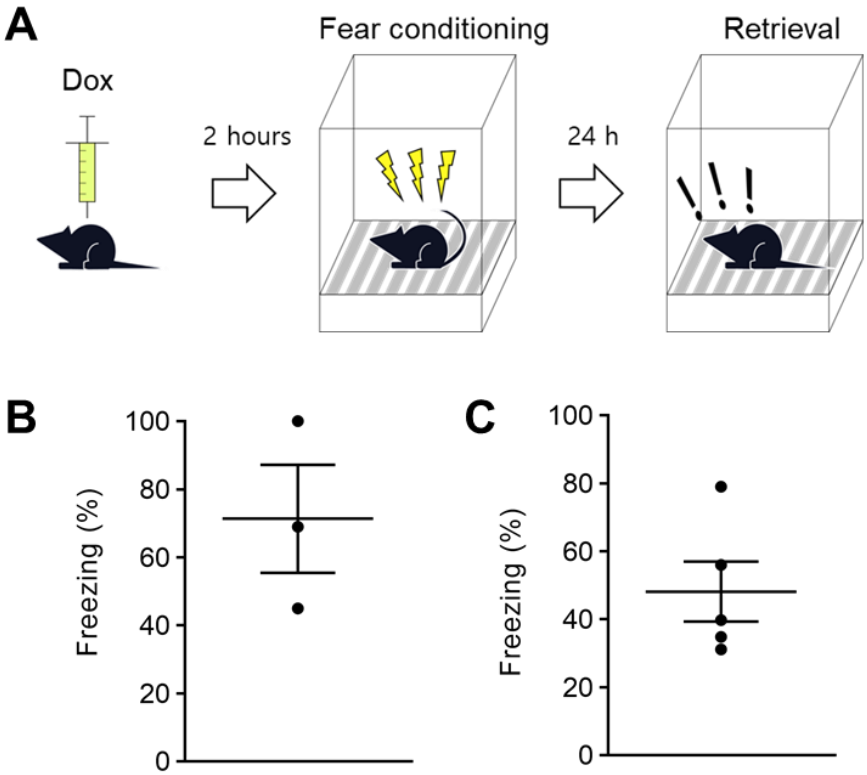

Figure 13. Contextual fear conditioning produce fear memory in mouse.

(A) Experimental procedure for contextual fear conditioning.

(B) Freezing levels in mice used for astrocyte-eGRASP density analysis. n = 3. Data are represented as the mean ± SEM.

(C) Freezing levels in the mice used for dendritic spine morphology analysis. n = 5. Data are represented as the mean ± SEM.

To analyze the astrocytic interaction to engram neurons, AAVs were injected into hippocampus to express astrocyte-eGRASP and neuronal eGRASP and to label engram neurons with fos promoter-driven tetTag sytem (Fig. 14A). The density of astrocyte-eGRASP and CA3-CA1 neuronal eGRASP was measured in engram neurons and neighboring nonengram neurons of hippocampal CA1 within each astrocyte territory (Fig. 14B). Surprisingly, engram neurons showed significantly higher density of astrocyte-eGRASP on their dendrite than nonengram neurons (Fig. 14C). It provides evidence that astrocyte is discriminating engram neurons to nonengram neurons, possibly regulating engram neuron specifically in unknown mechanism. Cyan eGRASP on engram and nonengram dendrite did not show statistical difference (Fig. 13C), confirming that eGRASP expression level was not the factor for the astrocyte-eGRASP difference.

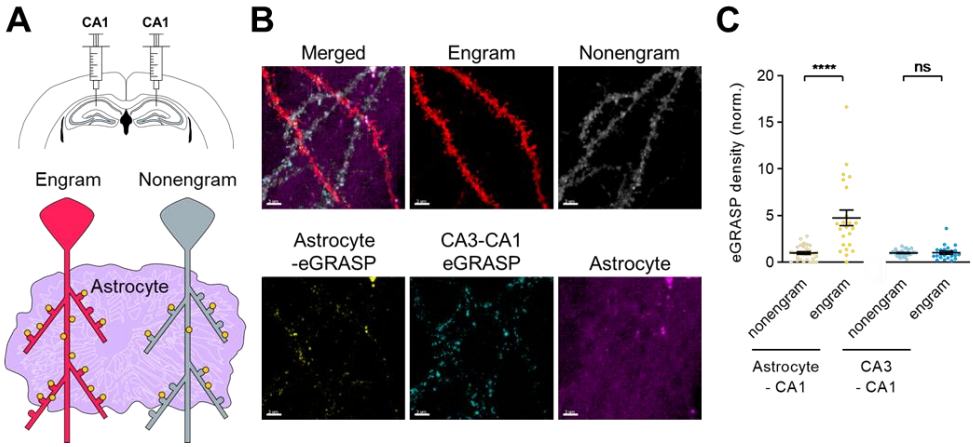

(Collaborated with Dr. Ji-il Kim, Dr. Dong Il Choi)

Figure 14. Astrocyte make more connection with engram neurons than nonengram neurons.

(A) Injection site and schematic illustration for engram dendrite (red) and nonengram dendrite (grey) with astrocyte-eGRASP (yellow).

(B) Representative images for astrocyte-eGRASP and CA3-CA1 neuronal eGRASP on engram and nonengram neurons. Scale bar, 5 μm.

(C) Engram neurons have more astrocyte contact than nonengram neurons after learning. Nonengram dendrite, n = 30; engram dendrite, n = 23. Mann-Whitney two-tailed test. n.s., not significant, ****$p < 0.0001$. Data are represented as mean ± SEM.

To find out the functional relevance of astrocytic contact, it was tested whether the morphology of dendritic spine with and without astrocyte-eGRASP differ (Fig. 15A, B). For the measurement, dendritic spines were reconstructed in 3D, and parameters such as the spine volume, spine head volume, spine head diameter and spine length were observed. Then, spines were categorized by the existence of astrocyte-eGRASP signal. Dendritic spine with astrocyte-eGRASP showed significantly larger morphology than the spine without astrocyte-eGRASP, in both engram and nonengram dendrites (Fig. 15C), consistent with previous report that spines with greater morphology have more stable astrocyte contact (Haber et al., 2006).

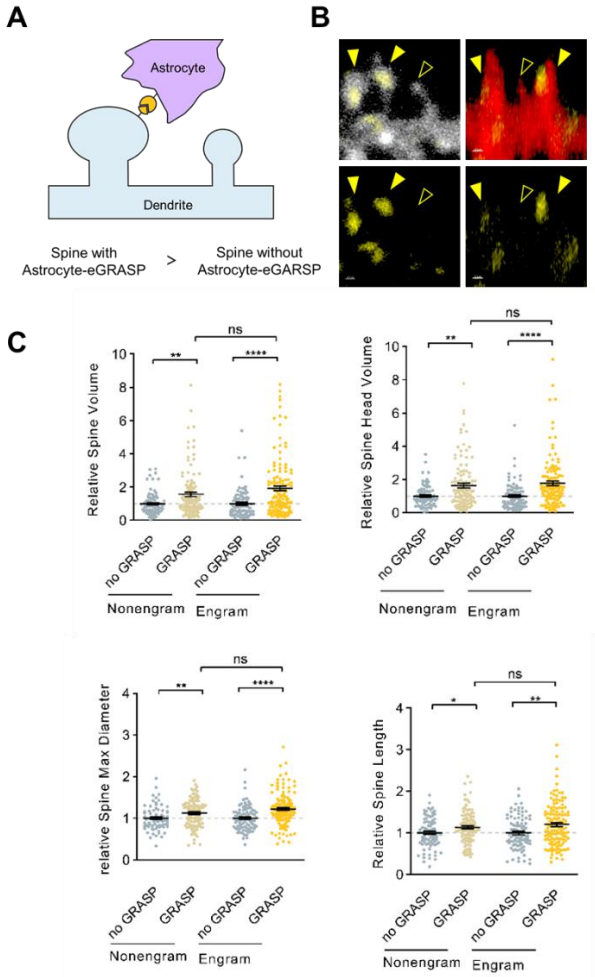

Figure 15. Dendritic spine with astrocytic connection exhibit larger morphology.

(A) Schematic illustration for dendritic spine with or without astrocyte-eGRASP.

(B) Representative images for dendritic spines with (filled arrow) or without (empty arrow) astrocyte-eGRASP (yellow) in nonengram (grey) and engram neurons (red). Scale bar, 0.3 μm.

(C) Dendritic spines with astrocyte-eGRASP have larger morphology. Nonengram, no eGRASP spine, n = 84; nonengram, eGRASP spine, n = 114; engram, no eGRASP spine, n = 93; engram, eGRASP spine, n =131. Mann-Whitney two-tailed test. n.s., not significant, **$p < 0.01$, ****$p < 0.0001$. Data are represented as mean ± SEM.

It is known that engram neurons are activated during learning (Ghandour et al., 2019), and neuronal activity can regulate astrocytic motility (Bernardinelli et al., 2014). To find out whether neuronal activity can affect the astrocyte-eGRASP density change, astrocyte-eGRASP was expressed in the primary astrocyte-primary neuron co-culture to visualize astrocyte-neuron connection. Then, neuronal activity was increased by reducing inhibitory tone using $GABA_A$ receptor antagonist bicuculline. Astrocyte-eGRASP disappearance and appearance were measured in 1-hour time interval before and after the application of bicuculline (Fig. 16A). It was found that disappearance of astrocyte-eGRASP was decreased after the application of bicuculline (Fig. 16B), while appearance did not show statistical difference before and after the bicuculline application (Fig. 16C). This result suggests that increased neuronal activity stabilizes the astrocytic connection, which may be involved in the increased astrocytic contact on the engram neuron.

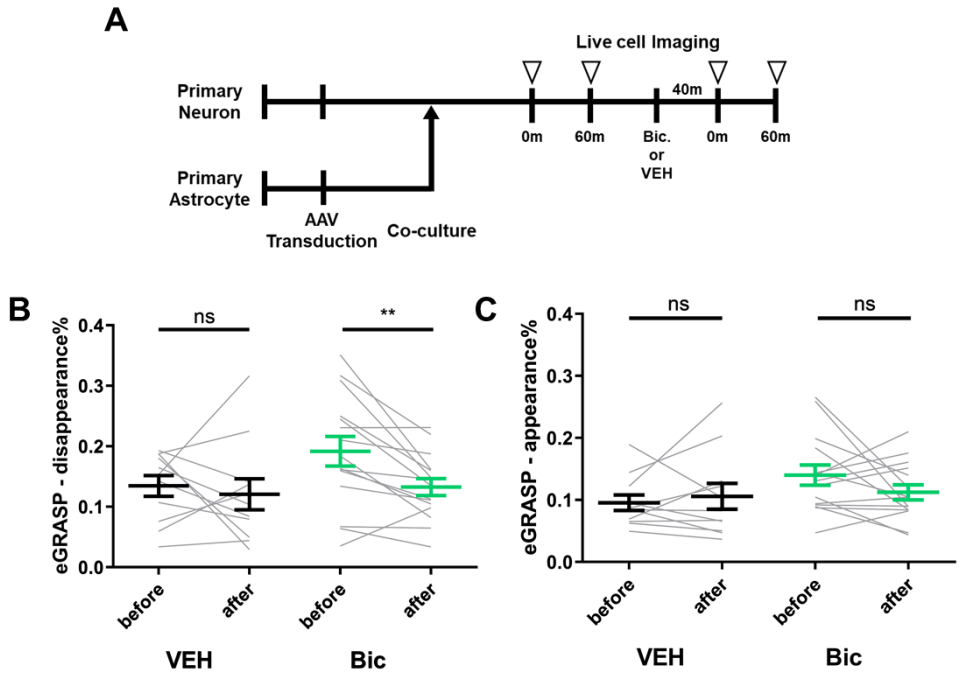

Figure 16. Increasing neuronal activity stabilizes astrocytic connection.

(A) Experimental procedure for the experiment.

(B, C) Disappearance (B) and appearance (C) of astrocyte-eGRASP before and after the drug application. VEH for the vehicle-treated group and Bic for the bicuculline-treated group. Vehicle, n = 11; Bicuculline, n = 15. Two-tailed paired t-test. n.s., not significant; **$p < 0.01$.

Next, it was questioned whether the increased astrocyte-eGRASP on engram neurons is dependent on the memory state. Therefore, the memory extinction paradigm was chosen to change the memory state, in which memory is extinguished when the mouse is repeatedly exposed to the conditioned stimuli (context). To test the effect of extinction, three behavioral groups were made: CFC-only, extinction and homecage group (Fig. 17A). CFC-only group was tested for fear memory and sacrificed a day after contextual fear conditioning. Extinction group went through 2 days of extinction session after fear conditioning, while homecage group stayed in the homecages. Then, extinction and homecage group was tested for fear memory and was sacrificed. As a result, the freezing level was significantly lower in the extinction group at the last retrieval test, while the fear memory was retained in CFC-only or homecage group (Fig. 17B).

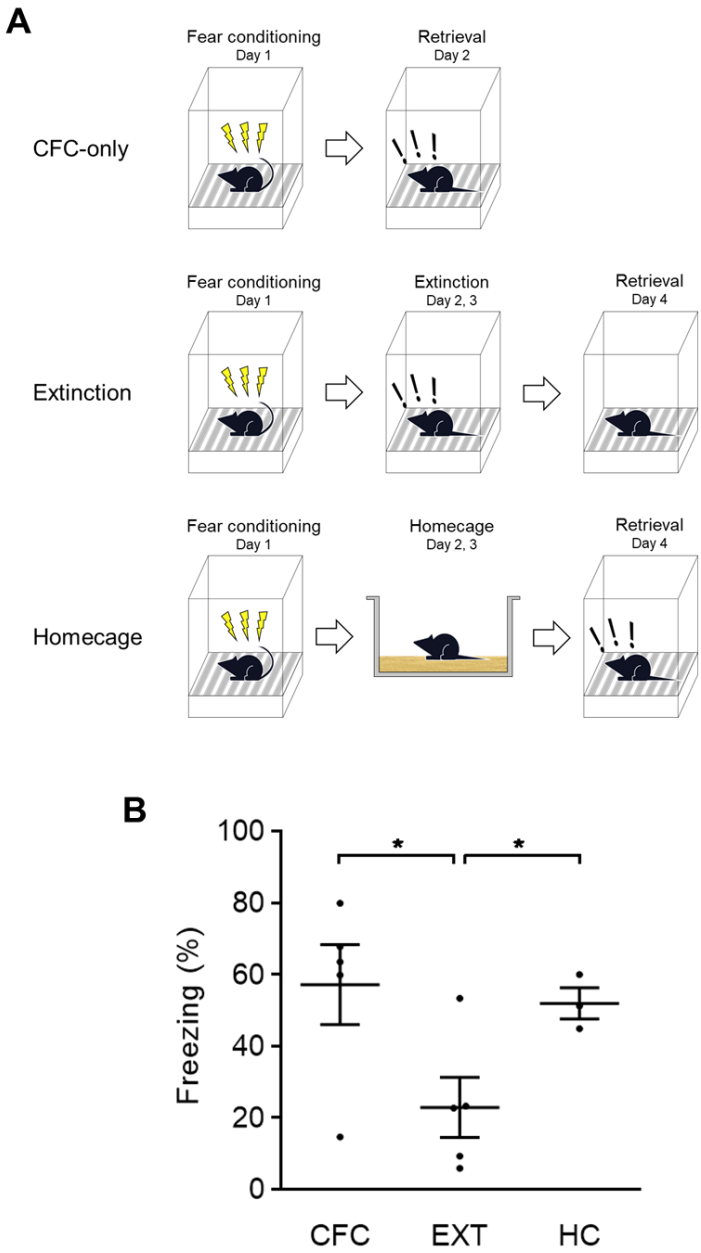

Figure 17. Extinction decreases fear memory in mouse.

(A) Experimental procedure for contextual fear conditioning and extinction.

(B) Freezing levels of last 5-minute retrieval in mice used for fear extinction experiment. CFC-only, n = 5; Extinction, n = 5; Homecage, n = 3. Unpaired t-test. *$p < 0.05$. Data are represented as the mean ± SEM.

Astrocyte-eGRASP density on engram and nonengram neurons were measured in CFC-only, extinction and homecage groups (Fig. 18A, B). Consistent with Fig. 14, the density of astrocyte-eGRASP on engram neurons were significantly higher compared to the eGRASP density on nonengram neurons in CFC-only group (Fig. 18C). Interestingly, astrocyte-eGRASP density on engram and nonengram neurons did not show significant difference in extinction group, while increased astrocyte-eGRASP density in engram neurons was persistent at the homecage group with retained fear memory (Fig. 18C). Persistent pattern of increased astrocyte-eGRASP on engram neurons in both CFC-only and homecage group show that the reversed astrocyte-eGRASP density on engram neurons in extinction group is due to the state of memory, but not the passage of time. Moreover, relative astrocyte-eGRASP density on engram neurons in extinction group was significantly lower than that of CFC-only and homecage groups. These results strongly support that astrocyte contact on engram neurons is corresponding to the state of memory.

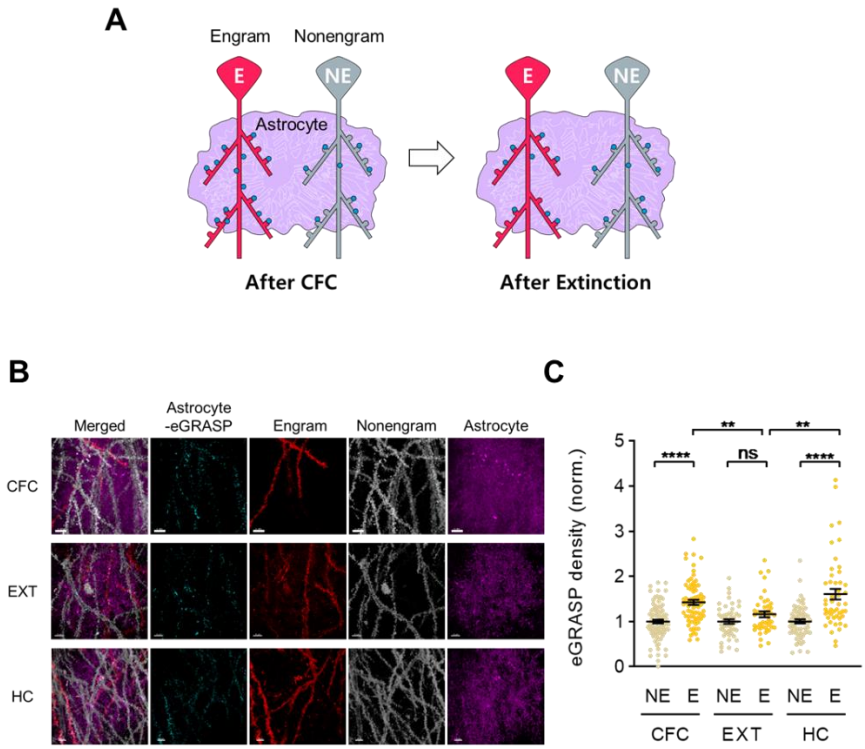

Figure 18. Memory extinction reverses increased astrocytic connection to engram neurons.

(A) Schematic illustration for engram dendrite and nonengram dendrite with astrocyte-eGRASP (cyan) after contextual fear conditioning and extinction.

(B) Representative images for astrocyte-eGRASP on engram and nonengarm dendrites in fear extinction experiment. Scale bar, 5 μm for CFC and 4 μm for extinction and homcage group.

(C) Increased astrocyte-eGRASP on engram neurons after fear conditioning is reversed after fear extinction. CFC group, nonengram dendrite, n = 85; CFC group, engram dendrite, n = 73; Extinction group, nonengram dendrite, n = 48; Extinction group, engram dendrite, n = 42; Homecage group, nonengram dendrite, n = 62; Homecage group, engram dendrite, n = 49. Mann-Whitney two-tailed test. n.s., not significant, **$p < 0.01$, ****$p < 0.0001$. Data are represented as mean ± SEM.

4.4. Discussion

In this chapter, it was revealed that astrocytes exhibit increased contact to memory-encoding engram neurons after learning (Fig. 19). Using astrocyte-eGRASP, it was able to identify astrocyte contact to engram neurons and compare it with the contact to random population of nonengram neurons within each astrocyte territory. Engram neuron is known to show increased activity during learning (Ghandour et al., 2019), and in this chapter it was shown that increasing neuronal activity stabilizes astrocyte contact, which may be the mechanism of increased astrocyte contact on engram neurons. Also, dendritic spine with astrocyte contact showed enlarged spine morphology, suggesting that astrocyte contact is involved in the synaptic potentiation of synapses. Lastly, astrocyte-engram neuron connection was measured after the extinction of memory, which revealed that the density of astrocyte-eGRASP on engram neurons is correlated to the state of the memory. Taken together, these results provide correlational evidence that astrocyte contact to engram neurons is involved in memory processing.

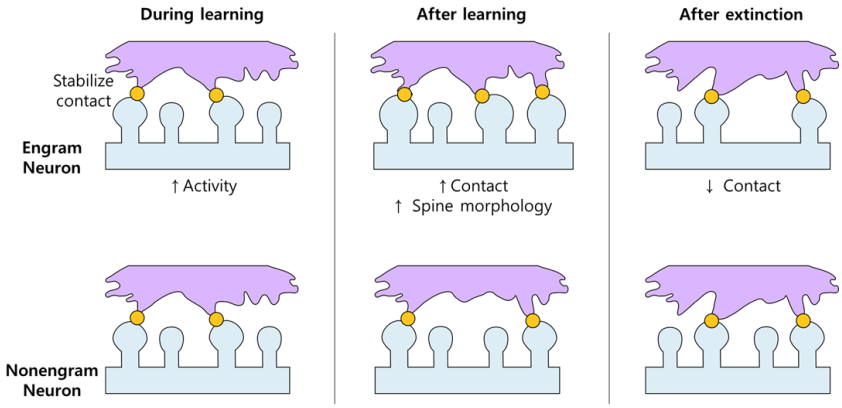

Figure 19. Model for learning-induced changes for astrocyte-neuron connection. (Left) During learning, activity of engram neurons may stabilize the neighboring astrocyte process. (Middle) After learning, stabilized astrocyte process results in increased astrocyte connection to engram neurons. Dendritic spine morphology is larger with astrocyte connection. (Right) After memory extinction, astrocyte-neuron connection density is similar in engram and nonengram dendrites.

The finding that astrocytes form engram neuron-specific connection pattern after learning provides structural evidence to astrocyte-mediated cognitive modulation. Astrocyte-released molecules, for example, D-serine in hippocampus, can modulate potentiation in nearby synapses (Henneberger et al., 2010) and is involved in cognition (Adamsky et al., 2018). However, without geometrical information, it was unclear how memory-related molecules would be delivered to engram neurons. The results in this chapter indicate that astrocytes establish specific contact pattern to the neurons participating in cognitive function, that may facilitate precise delivery of the released molecules.

It was also shown that astrocyte change the contact pattern according to the memory updating. In previous study, astrocyte D-serine release during memory acquisition was shown to be crucial for memory updating that happened days after the acquisition (Koh et al., 2022), but it was not clarified how molecular release during acquisition could affect the flexibility after long time. Combined with previous study, the result of structural examinations using astrocyte-eGRASP propose that changes in the astrocyte-engram neuron connection that are made during the memory acquisition may be important for the memory updating afterwards. Future study has to be done to identify whether the learning-induced gliotransmitter release may affect the astrocyte-neuron contact structure during memory acquisition and the memory updating.

It was shown that dendritic spines with astrocyte contact are larger. It is consistent with previous report that spines with larger volume tends to show more stable contact with astrocyte (Haber et al., 2006), although there is also contradictory reports reporting tight astrocyte connection to thin spines (Medvedev et al., 2014). Considering that large dendritic spines are signs of potentiation (Fortin et al., 2010;

Yang et al., 2008), it is conceivable that astrocyte may contribute to synaptic potentiation or maintenance of potentiated synapses. Indeed, increased astrocyte coverage of dendritic spine was reported after LTP induction (Bernardinelli et al., 2014). Future studies could delineate the role of astrocyte coverage on dendritic spines.

Interestingly, astrocyte contact to dendritic spine was related to the increased spine morphology in both engram and nonengram dendrites. It could be further questioned whether the increase of dendritic spines has causal relationship with the learning. If increased dendritic morphology in both engram and nonengram dendrites are caused by learning, it could be interpreted as the structural indication of hetero-neuronal plasticity or metaplasticity. Adding to the previous report that astrocytes are involved in hetero-neuronal plasticity (Martin et al., 2015), it has been proposed astrocytes are involved in heterosynaptic metaplasticity (Jones, 2015; Jones et al., 2013). Astrocyte-mediated metaplasticity could be related to the structural characteristics observed in this thesis, which could be related to cognitive functions such as memory updating.

CHAPTER V

Conclusion

5. Conclusion

To understand the role of astrocyte in synaptic communication and cognition, it is crucial to identify the structure of astrocyte-neuron contacts. In this thesis, astrocyte-eGRASP was developed, a tool that can visualize astrocyte-neuron contacts with fluorescence. Using astrocyte-eGRASP, astrocyte-neuron contacts can be observed both in vitro and in vivo, reflecting various types of astrocyte-neuron contacts. Astrocyte-eGRASP enabled the measurement of the astrocyte contact to memory-encoding engram neurons. It was revealed that astrocyte contact is increased in engram neurons after learning. In addition, when the memory underwent extinction, astrocyte contact with engram neurons was reversed to control levels.

In Chapter II, the novel technique called astrocyte-eGRASP was developed, that can label astrocyte-neuron contact with reconstituted eGRASP. The technique was tested using fluorescence imaging in vitro and in vivo. Astrocyte-eGRASP labeled the interface between astrocyte and neuron, and the labeling was reversible. Using immunogold-labeled electron microscopy, it was confirmed that astrocyte-eGRASP is reconstituted at astrocyte-neuron interface.

In Chapter III, different types of connections in single astrocyte territory was visualized using astrocyte-eGRASP. Firstly, the astrocyte connection to excitatory and inhibitory dendrite was visualized within single astrocyte territory. Secondly, astrocyte-axon and astrocyte-dendrite connection was visualized with different-colored astrocyte-eGRASP in single astrocyte, confirming that astrocytes make connection with different compartments of neuron. Moreover, in astrocyte-dendrite interaction, astrocyte exhibited coverage of both dendritic spines and dendritic shafts, and it was discovered that the ratio of dendritic shaft coverage is

different in dendritic trunk and secondary/tertiary dendrite. Lastly, astrocyte-eGRASP was demonstrated to be colocalized to various synaptic and functional proteins.

In Chapter IV, astrocyte connection to memory-encoding engram neurons was identified using astrocyte-eGRASP in different memory state. After learning, astrocyte connection to engram dendrites were denser than connection to neighboring nonengram dendrites in single astrocyte territory, while the density of connection to engram dendrites were reduced to the control level after memory extinction. Also, the morphology of dendritic spines was larger with astrocyte contacts. It was shown that astrocyte connection is stabilized after the increased neuronal activity in culture system.

Astrocytes participate in cognitive function (Adamsky et al., 2018; Kol et al., 2020) and interact with different type of neurons (Khakh, 2019; Mederos and Perea, 2019; Octeau et al., 2018). However, the structural basis of astrocytic regulation on cognitive function has not been clearly described. This study provides new technique that can visualize different types of connection within single astrocyte territory. Using the tool, novel finding was made that astrocyte show distinct connection pattern to memory-encoding engram neurons after learning. Combined with observation of astrocyte-neuron contact dynamics in culture system and memory extinction paradigm, it is proposed that astrocyte contacts to engram neurons are determined by neuronal activity and the state of memory. Further study would be required to elucidate the physiological role of the astrocyte-engram contact, which may reveal the novel mechanism of astrocyte participation in cognitive function.

Bibliography

Adamsky, A., Kol, A., Kreisel, T., Doron, A., Ozeri-Engelhard, N., Melcer, T., Refaeli, R., Horn, H., Regev, L., Groysman, M., *et al.* (2018). Astrocytic Activation Generates De Novo Neuronal Potentiation and Memory Enhancement. Cell *174*, 59-71 e14.

An, B., Kim, J., Park, K., Lee, S., Song, S., and Choi, S. (2017). Amount of fear extinction changes its underlying mechanisms. Elife *6*.

Araque, A., Parpura, V., Sanzgiri, R.P., and Haydon, P.G. (1999). Tripartite synapses: glia, the unacknowledged partner. Trends Neurosci *22*, 208-215.

Arizono, M., Inavalli, V., Panatier, A., Pfeiffer, T., Angibaud, J., Levet, F., Ter Veer, M.J.T., Stobart, J., Bellocchio, L., Mikoshiba, K., *et al.* (2020). Structural basis of astrocytic Ca(2+) signals at tripartite synapses. Nat Commun *11*, 1906.

Ashhad, S., and Narayanan, R. (2016). Active dendrites regulate the impact of gliotransmission on rat hippocampal pyramidal neurons. Proc Natl Acad Sci U S A *113*, E3280-3289.

Aten, S., Kiyoshi, C.M., Arzola, E.P., Patterson, J.A., Taylor, A.T., Du, Y., Guiher, A.M., Philip, M., Camacho, E.G., Mediratta, D., *et al.* (2022). Ultrastructural view of astrocyte arborization, astrocyte-astrocyte and astrocyte-synapse contacts, intracellular vesicle-like structures, and mitochondrial network. Prog Neurobiol *213*, 102264.

Badia-Soteras, A., Heistek, T.S., Kater, M.S.J., Mak, A., Negrean, A., van den Oever, M.C., Mansvelder, H.D., Khakh, B.S., Min, R., Smit, A.B., *et al.* (2022). Retraction of Astrocyte Leaflets From the Synapse Enhances Fear Memory. Biol Psychiatry.

Bakker, A., Kirwan, C.B., Miller, M., and Stark, C.E. (2008). Pattern separation in the human hippocampal CA3 and dentate gyrus. Science *319*, 1640-1642.

Bazargani, N., and Attwell, D. (2016). Astrocyte calcium signaling: the third wave. Nat Neurosci *19*, 182-189.

Bergersen, L.H. (2007). Is lactate food for neurons? Comparison of monocarboxylate transporter subtypes in brain and muscle. Neuroscience *145*, 11-19.

Bergersen, L.H., Magistretti, P.J., and Pellerin, L. (2005). Selective postsynaptic co-localization of MCT2 with AMPA receptor GluR2/3 subunits at excitatory synapses exhibiting AMPA receptor trafficking. Cereb Cortex

15, 361-370.

Bernardinelli, Y., Randall, J., Janett, E., Nikonenko, I., Konig, S., Jones, E.V., Flores, C.E., Murai, K.K., Bochet, C.G., Holtmaat, A.*, et al.* (2014). Activity-dependent structural plasticity of perisynaptic astrocytic domains promotes excitatory synapse stability. Curr Biol *24*, 1679-1688.

Bi, G.Q., and Poo, M.M. (1998). Synaptic modifications in cultured hippocampal neurons: dependence on spike timing, synaptic strength, and postsynaptic cell type. J Neurosci *18*, 10464-10472.

Bliss, T.V., and Lomo, T. (1973). Long-lasting potentiation of synaptic transmission in the dentate area of the anaesthetized rabbit following stimulation of the perforant path. J Physiol *232*, 331-356.

Borgdorff, A.J., and Choquet, D. (2002). Regulation of AMPA receptor lateral movements. Nature *417*, 649-653.

Bourne, J.N., and Harris, K.M. (2011). Coordination of size and number of excitatory and inhibitory synapses results in a balanced structural plasticity along mature hippocampal CA1 dendrites during LTP. Hippocampus *21*, 354-373.

Brunskine, C., Passlick, S., and Henneberger, C. (2022). Structural Heterogeneity of the GABAergic Tripartite Synapse. Cells *11*.

Bushong, E.A., Martone, M.E., Jones, Y.Z., and Ellisman, M.H. (2002). Protoplasmic astrocytes in CA1 stratum radiatum occupy separate anatomical domains. J Neurosci *22*, 183-192.

Choi, D.I., Kim, J., Lee, H., Kim, J.I., Sung, Y., Choi, J.E., Venkat, S.J., Park, P., Jung, H., and Kaang, B.K. (2021). Synaptic correlates of associative fear memory in the lateral amygdala. Neuron *109*, 2717-2726 e2713.

Choi, J.H., Sim, S.E., Kim, J.I., Choi, D.I., Oh, J., Ye, S., Lee, J., Kim, T., Ko, H.G., Lim, C.S.*, et al.* (2018). Interregional synaptic maps among engram cells underlie memory formation. Science *360*, 430-435.

Christopherson, K.S., Ullian, E.M., Stokes, C.C., Mullowney, C.E., Hell, J.W., Agah, A., Lawler, J., Mosher, D.F., Bornstein, P., and Barres, B.A. (2005). Thrombospondins are astrocyte-secreted proteins that promote CNS synaptogenesis. Cell *120*, 421-433.

Doron, A., Rubin, A., Benmelech-Chovav, A., Benaim, N., Carmi, T., Refaeli, R., Novick, N., Kreisel, T., Ziv, Y., and Goshen, I. (2022). Hippocampal astrocytes encode reward location. Nature *609*, 772-778.

Engert, F., and Bonhoeffer, T. (1999). Dendritic spine changes associated

with hippocampal long-term synaptic plasticity. Nature *399*, 66-70.

Fodstad, H. (2002). The neuron saga. International Congress Series *1247*, 645-650.

Fortin, D.A., Davare, M.A., Srivastava, T., Brady, J.D., Nygaard, S., Derkach, V.A., and Soderling, T.R. (2010). Long-term potentiation-dependent spine enlargement requires synaptic Ca2+ -permeable AMPA receptors recruited by CaM-kinase I. J Neurosci *30*, 11565-11575.

Gao, V., Suzuki, A., Magistretti, P.J., Lengacher, S., Pollonini, G., Steinman, M.Q., and Alberini, C.M. (2016). Astrocytic beta2-adrenergic receptors mediate hippocampal long-term memory consolidation. Proc Natl Acad Sci U S A *113*, 8526-8531.

Gavrilov, N., Golyagina, I., Brazhe, A., Scimemi, A., Turlapov, V., and Semyanov, A. (2018). Astrocytic Coverage of Dendritic Spines, Dendritic Shafts, and Axonal Boutons in Hippocampal Neuropil. Front Cell Neurosci *12*, 248.

Ghandour, K., Ohkawa, N., Fung, C.C.A., Asai, H., Saitoh, Y., Takekawa, T., Okubo-Suzuki, R., Soya, S., Nishizono, H., Matsuo, M.*, et al.* (2019). Orchestrated ensemble activities constitute a hippocampal memory engram. Nat Commun *10*, 2637.

Golgi, C. (1906). The neuron doctrine - theory and facts (Nobel lecture: NobelPrize.org).

Grossen, N.E., and Kelley, M.J. (1972). Species-specific behavior and acquisition of avoidance behavior in rats. J Comp Physiol Psychol *81*, 307-310.

Haber, M., Zhou, L., and Murai, K.K. (2006). Cooperative astrocyte and dendritic spine dynamics at hippocampal excitatory synapses. J Neurosci *26*, 8881-8891.

Halassa, M.M., Fellin, T., Takano, H., Dong, J.H., and Haydon, P.G. (2007). Synaptic islands defined by the territory of a single astrocyte. J Neurosci *27*, 6473-6477.

Han, J.H., Kushner, S.A., Yiu, A.P., Cole, C.J., Matynia, A., Brown, R.A., Neve, R.L., Guzowski, J.F., Silva, A.J., and Josselyn, S.A. (2007). Neuronal competition and selection during memory formation. Science *316*, 457-460.

Han, J.H., Kushner, S.A., Yiu, A.P., Hsiang, H.L., Buch, T., Waisman, A., Bontempi, B., Neve, R.L., Frankland, P.W., and Josselyn, S.A. (2009). Selective erasure of a fear memory. Science *323*, 1492-1496.

Hebb, D.O. (1949). The organization of behavior; a neuropsychological theory (New York,: Wiley).

Henneberger, C., Papouin, T., Oliet, S.H., and Rusakov, D.A. (2010). Long-term potentiation depends on release of D-serine from astrocytes. Nature *463*, 232-236.

Ishizuka, N., Weber, J., and Amaral, D.G. (1990). Organization of intrahippocampal projections originating from CA3 pyramidal cells in the rat. J Comp Neurol *295*, 580-623.

Jeong, Y., Cho, H.Y., Kim, M., Oh, J.P., Kang, M.S., Yoo, M., Lee, H.S., and Han, J.H. (2021). Synaptic plasticity-dependent competition rule influences memory formation. Nat Commun *12*, 3915.

Jones, O.D. (2015). Astrocyte-mediated metaplasticity in the hippocampus: Help or hindrance? Neuroscience *309*, 113-124.

Jones, O.D., Hulme, S.R., and Abraham, W.C. (2013). Purinergic receptor- and gap junction-mediated intercellular signalling as a mechanism of heterosynaptic metaplasticity. Neurobiol Learn Mem *105*, 31-39.

Josselyn, S.A., Kohler, S., and Frankland, P.W. (2015). Finding the engram. Nat Rev Neurosci *16*, 521-534.

Josselyn, S.A., and Tonegawa, S. (2020). Memory engrams: Recalling the past and imagining the future. Science *367*.

Kajiwara, R., Wouterlood, F.G., Sah, A., Boekel, A.J., Baks-te Bulte, L.T., and Witter, M.P. (2008). Convergence of entorhinal and CA3 inputs onto pyramidal neurons and interneurons in hippocampal area CA1--an anatomical study in the rat. Hippocampus *18*, 266-280.

Khakh, B.S. (2019). Astrocyte-Neuron Interactions in the Striatum: Insights on Identity, Form, and Function. Trends Neurosci *42*, 617-630.

Klatt, O., Repetto, D., Brockhaus, J., Reissner, C., El Khallouqi, A., Rohlmann, A., Heine, M., and Missler, M. (2021). Endogenous beta-neurexins on axons and within synapses show regulated dynamic behavior. Cell Rep *35*, 109266.

Koh, W., Park, M., Chun, Y.E., Lee, J., Shim, H.S., Park, M.G., Kim, S., Sa, M., Joo, J., Kang, H.*, et al.* (2022). Astrocytes Render Memory Flexible by Releasing D-Serine and Regulating NMDA Receptor Tone in the Hippocampus. Biol Psychiatry *91*, 740-752.

Kol, A., Adamsky, A., Groysman, M., Kreisel, T., London, M., and Goshen, I. (2020). Astrocytes contribute to remote memory formation by modulating hippocampal-cortical communication during learning. Nat Neurosci *23*, 1229-

1239.

Kruyer, A., Angelis, A., Garcia-Keller, C., Li, H., and Kalivas, P.W. (2022). Plasticity in astrocyte subpopulations regulates heroin relapse. Sci Adv *8*, eabo7044.

Lee, C., Lee, B.H., Jung, H., Lee, C., Sung, Y., Kim, H., Kim, J., Shim, J.Y., Kim, J.I., Choi, D.I.*, et al.* (2022). Hippocampal engram networks for fear memory recruit new synapses and modify pre-existing synapses in vivo. Curr Biol.

Lee, J.H., Kim, J.Y., Noh, S., Lee, H., Lee, S.Y., Mun, J.Y., Park, H., and Chung, W.S. (2021). Astrocytes phagocytose adult hippocampal synapses for circuit homeostasis. Nature *590*, 612-617.

Lei, Z., Xie, L., Li, C.H., Lam, Y.Y., Ramkrishnan, A.S., Fu, Z., Zeng, X., Liu, S., Iqbal, Z., and Li, Y. (2022). Chemogenetic Activation of Astrocytes in the Basolateral Amygdala Contributes to Fear Memory Formation by Modulating the Amygdala-Prefrontal Cortex Communication. Int J Mol Sci *23*.

Lezmy, J., Arancibia-Carcamo, I.L., Quintela-Lopez, T., Sherman, D.L., Brophy, P.J., and Attwell, D. (2021). Astrocyte Ca(2+)-evoked ATP release regulates myelinated axon excitability and conduction speed. Science *374*, eabh2858.

Li, Y., Li, L., Wu, J., Zhu, Z., Feng, X., Qin, L., Zhu, Y., Sun, L., Liu, Y., Qiu, Z.*, et al.* (2020). Activation of astrocytes in hippocampus decreases fear memory through adenosine A1 receptors. Elife *9*.

Liu, X., Ramirez, S., Pang, P.T., Puryear, C.B., Govindarajan, A., Deisseroth, K., and Tonegawa, S. (2012). Optogenetic stimulation of a hippocampal engram activates fear memory recall. Nature *484*, 381-385.

Lushnikova, I., Skibo, G., Muller, D., and Nikonenko, I. (2009). Synaptic potentiation induces increased glial coverage of excitatory synapses in CA1 hippocampus. Hippocampus *19*, 753-762.

MacDonald, C.J., Carrow, S., Place, R., and Eichenbaum, H. (2013). Distinct hippocampal time cell sequences represent odor memories in immobilized rats. J Neurosci *33*, 14607-14616.

Madar, A.D., Ewell, L.A., and Jones, M.V. (2019). Pattern separation of spiketrains in hippocampal neurons. Sci Rep *9*, 5282.

Maren, S. (2001). Neurobiology of Pavlovian fear conditioning. Annu Rev Neurosci *24*, 897-931.

Markram, H., Lubke, J., Frotscher, M., and Sakmann, B. (1997). Regulation of synaptic efficacy by coincidence of postsynaptic APs and EPSPs. Science *275*,

213-215.

Martin-Fernandez, M., Jamison, S., Robin, L.M., Zhao, Z., Martin, E.D., Aguilar, J., Benneyworth, M.A., Marsicano, G., and Araque, A. (2017). Synapse-specific astrocyte gating of amygdala-related behavior. Nat Neurosci *20*, 1540-1548.

Martin, R., Bajo-Graneras, R., Moratalla, R., Perea, G., and Araque, A. (2015). Circuit-specific signaling in astrocyte-neuron networks in basal ganglia pathways. Science *349*, 730-734.

Mason, S. (2017). Lactate Shuttles in Neuroenergetics-Homeostasis, Allostasis and Beyond. Front Neurosci *11*, 43.

Matos, M., Bosson, A., Riebe, I., Reynell, C., Vallee, J., Laplante, I., Panatier, A., Robitaille, R., and Lacaille, J.C. (2018). Astrocytes detect and upregulate transmission at inhibitory synapses of somatostatin interneurons onto pyramidal cells. Nat Commun *9*, 4254.

Matsuzaki, M., Ellis-Davies, G.C., Nemoto, T., Miyashita, Y., Iino, M., and Kasai, H. (2001). Dendritic spine geometry is critical for AMPA receptor expression in hippocampal CA1 pyramidal neurons. Nat Neurosci *4*, 1086-1092.

Mederos, S., and Perea, G. (2019). GABAergic-astrocyte signaling: A refinement of inhibitory brain networks. Glia *67*, 1842-1851.

Medvedev, N., Popov, V., Henneberger, C., Kraev, I., Rusakov, D.A., and Stewart, M.G. (2014). Glia selectively approach synapses on thin dendritic spines. Philos Trans R Soc Lond B Biol Sci *369*, 20140047.

Nagai, J., Rajbhandari, A.K., Gangwani, M.R., Hachisuka, A., Coppola, G., Masmanidis, S.C., Fanselow, M.S., and Khakh, B.S. (2019). Hyperactivity with Disrupted Attention by Activation of an Astrocyte Synaptogenic Cue. Cell *177*, 1280-1292 e1220.

Navarrete, M., and Araque, A. (2010). Endocannabinoids potentiate synaptic transmission through stimulation of astrocytes. Neuron *68*, 113-126.

Neunuebel, J.P., and Knierim, J.J. (2014). CA3 retrieves coherent representations from degraded input: direct evidence for CA3 pattern completion and dentate gyrus pattern separation. Neuron *81*, 416-427.

Nishizaki, T., Nagai, K., Nomura, T., Tada, H., Kanno, T., Tozaki, H., Li, X.X., Kondoh, T., Kodama, N., Takahashi, E.*, et al.* (2002). A new neuromodulatory pathway with a glial contribution mediated via A(2a) adenosine receptors. Glia *39*, 133-147.

O'Carroll, S.J., Cook, W.H., and Young, D. (2020). AAV Targeting of Glial Cell Types in the Central and Peripheral Nervous System and Relevance to Human Gene Therapy. Front Mol Neurosci *13*, 618020.

O'Keefe, J., and Dostrovsky, J. (1971). The hippocampus as a spatial map. Preliminary evidence from unit activity in the freely-moving rat. Brain Res *34*, 171-175.

Octeau, J.C., Chai, H., Jiang, R., Bonanno, S.L., Martin, K.C., and Khakh, B.S. (2018). An Optical Neuron-Astrocyte Proximity Assay at Synaptic Distance Scales. Neuron *98*, 49-66 e49.

Patrushev, I., Gavrilov, N., Turlapov, V., and Semyanov, A. (2013). Subcellular location of astrocytic calcium stores favors extrasynaptic neuron-astrocyte communication. Cell Calcium *54*, 343-349.

Pavlov, P.I. (2010). Conditioned reflexes: An investigation of the physiological activity of the cerebral cortex. Ann Neurosci *17*, 136-141.

Pelvig, D.P., Pakkenberg, H., Stark, A.K., and Pakkenberg, B. (2008). Neocortical glial cell numbers in human brains. Neurobiol Aging *29*, 1754-1762.

Perea, G., and Araque, A. (2007). Astrocytes potentiate transmitter release at single hippocampal synapses. Science *317*, 1083-1086.

Perea, G., Navarrete, M., and Araque, A. (2009). Tripartite synapses: astrocytes process and control synaptic information. Trends Neurosci *32*, 421-431.

Perez-Alvarez, A., Navarrete, M., Covelo, A., Martin, E.D., and Araque, A. (2014). Structural and functional plasticity of astrocyte processes and dendritic spine interactions. J Neurosci *34*, 12738-12744.

Pierre, K., and Pellerin, L. (2005). Monocarboxylate transporters in the central nervous system: distribution, regulation and function. J Neurochem *94*, 1-14.

Poldrack, R.A., and Packard, M.G. (2003). Competition among multiple memory systems: converging evidence from animal and human brain studies. Neuropsychologia *41*, 245-251.

Pregno, G., Frola, E., Graziano, S., Patrizi, A., Bussolino, F., Arese, M., and Sassoe-Pognetto, M. (2013). Differential regulation of neurexin at glutamatergic and GABAergic synapses. Front Cell Neurosci *7*, 35.

Quirk, G.J., and Mueller, D. (2008). Neural mechanisms of extinction learning and retrieval. Neuropsychopharmacology *33*, 56-72.

Ramirez, S., Liu, X., Lin, P.A., Suh, J., Pignatelli, M., Redondo, R.L., Ryan, T.J., and Tonegawa, S. (2013). Creating a false memory in the hippocampus. Science *341*, 387-391.

Reilly, J.E., Hanson, H.H., and Phillips, G.R. (2011). Persistence of excitatory shaft synapses adjacent to newly emerged dendritic protrusions. Mol Cell Neurosci *48*, 129-136.

Risher, W.C., Patel, S., Kim, I.H., Uezu, A., Bhagat, S., Wilton, D.K., Pilaz, L.J., Singh Alvarado, J., Calhan, O.Y., Silver, D.L.*, et al.* (2014). Astrocytes refine cortical connectivity at dendritic spines. Elife *3*.

Rollenhagen, A., Satzler, K., Rodriguez, E.P., Jonas, P., Frotscher, M., and Lubke, J.H. (2007). Structural determinants of transmission at large hippocampal mossy fiber synapses. J Neurosci *27*, 10434-10444.

Roy, D.S., Park, Y.G., Kim, M.E., Zhang, Y., Ogawa, S.K., DiNapoli, N., Gu, X., Cho, J.H., Choi, H., Kamentsky, L.*, et al.* (2022). Brain-wide mapping reveals that engrams for a single memory are distributed across multiple brain regions. Nat Commun *13*, 1799.

Schindelin, J., Arganda-Carreras, I., Frise, E., Kaynig, V., Longair, M., Pietzsch, T., Preibisch, S., Rueden, C., Saalfeld, S., Schmid, B.*, et al.* (2012). Fiji: an open-source platform for biological-image analysis. Nat Methods *9*, 676-682.

Schiweck, J., Eickholt, B.J., and Murk, K. (2018). Important Shapeshifter: Mechanisms Allowing Astrocytes to Respond to the Changing Nervous System During Development, Injury and Disease. Front Cell Neurosci *12*, 261.

Scoville, W.B., and Milner, B. (1957). Loss of recent memory after bilateral hippocampal lesions. J Neurol Neurosurg Psychiatry *20*, 11-21.

Sharma, V. (2018). ImageJ plugin HyperStackReg V5.6.

Shelkar, G.P., Liu, J., and Dravid, S.M. (2021). Astrocytic NMDA Receptors in the Basolateral Amygdala Contribute to Facilitation of Fear Extinction. Int J Neuropsychopharmacol *24*, 907-919.

Spacek, J. (1985). Three-dimensional analysis of dendritic spines. III. Glial sheath. Anat Embryol (Berl) *171*, 245-252.

Takacs, V.T., Freund, T.F., and Nyiri, G. (2013). Neuroligin 2 is expressed in synapses established by cholinergic cells in the mouse brain. PLoS One *8*, e72450.

Varoqueaux, F., Jamain, S., and Brose, N. (2004). Neuroligin 2 is exclusively localized to inhibitory synapses. Eur J Cell Biol *83*, 449-456.

Vazdarjanova, A., and Guzowski, J.F. (2004). Differences in hippocampal neuronal population responses to modifications of an environmental context: evidence for distinct, yet complementary, functions of CA3 and CA1 ensembles. J Neurosci *24*, 6489-6496.

Volterra, A., Liaudet, N., and Savtchouk, I. (2014). Astrocyte Ca(2)(+) signalling: an unexpected complexity. Nat Rev Neurosci *15*, 327-335.

Wheal, H.V., Lancaster, B., and Bliss, T.V. (1983). Long-term potentiation in Schaffer collateral and commissural systems of the hippocampus: in vitro study in rats pretreated with kainic acid. Brain Res *272*, 247-253.

Witcher, M.R., Kirov, S.A., and Harris, K.M. (2007). Plasticity of perisynaptic astroglia during synaptogenesis in the mature rat hippocampus. Glia *55*, 13-23.

Yang, J., Wang, L., Yang, F., Luo, H., Xu, L., Lu, J., Zeng, S., and Zhang, Z. (2013). mBeRFP, an improved large stokes shift red fluorescent protein. PLoS One *8*, e64849.

Yang, Y., Wang, X.B., Frerking, M., and Zhou, Q. (2008). Spine expansion and stabilization associated with long-term potentiation. J Neurosci *28*, 5740-5751.

Yu, X., Taylor, A.M.W., Nagai, J., Golshani, P., Evans, C.J., Coppola, G., and Khakh, B.S. (2018). Reducing Astrocyte Calcium Signaling In Vivo Alters Striatal Microcircuits and Causes Repetitive Behavior. Neuron *99*, 1170-1187 e1179.

Zhang, S.X., Rogulja, D., and Crickmore, M.A. (2016). Dopaminergic Circuitry Underlying Mating Drive. Neuron *91*, 168-181.

Zhou, Y., Won, J., Karlsson, M.G., Zhou, M., Rogerson, T., Balaji, J., Neve, R., Poirazi, P., and Silva, A.J. (2009). CREB regulates excitability and the allocation of memory to subsets of neurons in the amygdala. Nat Neurosci *12*, 1438-1443.

요약(국문초록)

기억은 엔그램(engram) 세포라고 불리는 신경세포의 일부 집단에 의하여 저장된다. 엔그램 세포는 기억을 저장하고, 재생하고, 업데이트하는 데에 관여한다. 최근 연구에서 신경세포 외에도 중추신경계의 교세포 중 하나인 성상교세포도 기억을 저장하는 데 주체적으로 기여한다는 것이 알려졌다. 하지만, 성상교세포가 기억 기능에 기여하기 위해 기억을 저장하는 엔그램 신경세포와 어떻게 상호 작용하는지는 기술적인 한계로 인해 확인되지 않았다. 본 연구는 astrocyte-eGRASP라고 불리는 형광 표지 기법을 새롭게 개발하여 성상교세포와 뉴런 간의 상호 작용을 확인하고자 하였다. 이 도구를 사용하여, 엔그램 신경세포에 대한 성상교세포의 특이적인 연결 패턴을 확인할 수 있었다. 학습 후, 기억을 저장하는 엔그램 신경세포에 대한 성상교세포 연결이 증가했다. 이에 비하여, 기억이 소멸(memory extinction)된 경우, 기억을 저장하는 엔그램 신경세포에 대한 성상교세포의 연결이 감소하였다. 즉, 기억 상태에 따라 성상교세포 연결이 달라짐을 보여주었다. 이러한 결과는 기억을 저장하는 엔그램 신경세포에 대한 성상교세포 연결이 기억 상태에 따라 조절된다는 것을 강하게 시사하며, 성상교세포가 기억을 조절하는 새로운 기작에 대한 가능성을 제시한다.

주요어: 기억, 성상교세포, 기억저장신경세포, 엔그램 세포, 시냅스
학번: 2018-21127